NTD Ge sensor development for superconducting bolometers

By

S. Mathimalar

PHYS01200904007

Bhabha Atomic Research Centre, Mumbai – 400 085

A thesis submitted to the

Board of Studies in Physical Sciences

In partial fulfillment of requirements

For the Degree of

DOCTOR OF PHILOSOPHY

of

HOMI BHABHA NATIONAL INSTITUTE

December, 2015

Homi Bhabha National Institute

Recommendations of the Viva Voce Board

As members of the Viva Voce Board, we certify that we have read the dissertation prepared by S. Mathimalar entitled "NTD Ge sensor development for superconducting bolometers" and recommend that it may be accepted as fulfilling the dissertation requirement for the Degree of Doctor of philosophy.

Chairman - Dr. G. Ravikumar **Date:**

Guide / Convener - Prof. R. G. Pillay **Date:**

Member - Prof. S. Ramakrishnan **Date:**

Member - Prof. A. A. Tulapurkar **Date:**

Member - Prof. V. Nanal **Date:**

Member - Prof. S. Banerjee **Date:**

Final approval and acceptance of this dissertation is contingent upon the candidate's submission of the final copies of the dissertation to HBNI.

I/We hereby certify that I/we have read this dissertation prepared under my/our direction and recommend that it may be accepted as fulfilling the dissertation requirement.

Date:

Place: **Guide**

STATEMENT BY AUTHOR

This dissertation has been submitted in partial fulfillment of requirements for an advanced degree at Homi Bhabha National Institute (HBNI) and is deposited in the Library to be made available to borrowers under rules of the HBNI.

Brief quotations from this dissertation are allowable without special permission, provided that accurate acknowledgement of source is made. Requests for permission for extended quotation from or reproduction of this manuscript in whole or in part may be granted by the Competent Authority of HBNI when in his or her judgement the proposed use of the material is in the interests of scholarship. In all other instances, however, permission must be obtained from the author.

S. Mathimalar

DECLARATION

I, hereby declare that the investigation presented in the thesis has been carried out by me. The work is original and has not been submitted earlier as a whole or in part for a degree / diploma at this or any other Institution / University.

S. Mathimalar

List of Publications arising from the thesis

Journal

1. "Study of radioactive impurities in neutron transmutation doped Ge", **S. Mathimalar**, N. Dokania, V. Singh, V. Nanal, R.G. Pillay, A. Shrivastava, V.M. Datar, K.C. Jagadeesan, S.V. Thakare, *Nuclear Instrumentation and Methods A*, **2015**, *774*, 68-73.

2. "Characterization of neutron transmutation doped (NTD) Ge for low temperature sensor development", **S. Mathimalar**, V. Singh, N. Dokania, V. Nanal, R. G. Pillay, S. Pal, S. Ramakrishnan, A. Shrivastava, Priya Maheswari, P. K. Pujari, S. Ojha, D. Kanjilal, K.C. Jagadeesan and S.V. Thakare, *Nuclear Instrumentation and Methods B*, **2015**, *345*, 33-36.

Conferences

1. "Development of NTD Ge sensors for low temperature thermometry", **S. Mathimalar**, V. Singh, N. Dokania, V. Nanal, R.G. Pillay, S. Pal, S. Ramakrishnan, A. Shrivastava, Priya Maheshwari, P.K. Pujari, S. Ojha, D. Kanjilal, K.C. Jagadeesan, and S.V. Thakare, *International Workshop on Low Temperature Electronics 2014, Proceedings of IEEE Explore, doi:10.1109/WOLTE.2014.6881014.*

Others

1. *Specific Heat of Teflon, Torlon - 4203 and Torlon - 4301 in the range of 30 - 400 mK*, V. Singh, A. Garai, **S. Mathimalar**, N. Dokania, V. Nanal, R. G. Pillay, S. Ramakrishnan, Cryogenics, 67, **2015**, 15.

2. *Heat capacity setup for superconducting bolometer absorbers below* 400*mK*, V. Singh, **S. Mathimalar**, N. Dokania, V. Nanal, R. G. Pillay, S. Ramakrishnan, Journal of Low Temperature Physics, 175, **2014**, 604.

3. *Study of neutron-induced background and its effect on the search of* $0\nu\beta\beta$ *decay in* ^{124}Sn, N. Dokania, V. Singh, **S. Mathimalar**, C. Ghosh, V. Nanal, R.G. Pillay, S. Pal, K.G. Bhushan and A. Shrivastava, *Journal of Instrumentation*, doi:10.1088/1748-0221/9/11/P11002.

4. *Characterization and modeling of a low background HPGe detector*, N. Dokania, V. Singh, **S. Mathimalar**, V. Nanal, S. Pal, R. G. Pillay, Nucl. Instr. and Meth. A, 745, **2014**, 119.

5. *Cryogen Free Dilution Refrigerator for bolometric search of neutrinoless double decay (*$0\nu\beta\beta$*) in* ^{124}*Sn*, V. Singh, **Mathimalar. S**, N. Dokania, V. Nanal, R. G. Pillay, S. Ramakrishnan, Pramana - Journal of Physics, 81, **2013**, 719.

S. Mathimalar

Dedicated to

My beloved teacher Ms. V. Bhanumathy

to my dear friend Ms. S. Brindha

and to my family

ACKNOWLEDGMENTS

For the completion of my thesis work, many individuals have supported in several ways. I would like to express my sincere gratitude to my advisor Prof. R.G. Pillay for his constant support throughout my Ph.D. research work, for listening to my ideas patiently, for correcting my ideas and for providing the freedom in the research work. He always welcomes innovative idea and ask me to think intuitively. The greatest thing I learned from my advisor is to learn things from the scratch, give one's complete involvement to work and enjoy whatever one does. My sincere thank to Prof. Vandana Nanal for always keeping me in track and one who taught me to write and think in a scientific way. Without her constant motivation, it would have been impossible to complete the thesis work in time. I thank my fellow labmates Dr. Y. Gowda, Vivek, Neha, Chandan and Abhijit for their company throughout my Ph.D. and for the various scientific discussions we made while trying to understand a concept. I would like to thank Prof. S. Ramakrishnan, Prof. Vivek Datar, Prof. Mandar Deshmukh, Prof. Kantimay Das Gupta, Prof. Pratap Raychaudhuri, Dr. G. Ravikumar, Dr. P.K. Pujari and Dr. Ashwin Tulapurkar for their valuable discussions and the suggestion obtained to carry out this thesis work. My sincere thanks to Mr. Jagadeesan for the irradiation of the Ge samples irradiated with the required neutron dose. I thank Dr. Priya Maheswari, Dr. Dinakar Kanjilal and Mr. Sunil Ojha for their contribution in the experimental work. I

acknowledge Dr. Madhavi, Sudipta, John, Sameer, Carina, R. Bapat and B.A. Chalke for their help while performing the experiment. I thank DNAP staff members Mr. M.S. Pose, Mr. J.N. Karande, Ms. Sadhana, Ms. Prajakta, Mr. K.S. Divekar, Mr. Mallikaarunachary for their support in the experimental work. I acknowledge central workshop for providing the necessary equipment/apparatus in time. I would like to thank TIFR Medical section for keeping me fit throughout my research work. I thank my friends and colleagues Meghna, Moon Moon, Lakshmi, Animesh, Ali Ajmi, Nitali, Sudeshna, Aswathi, Harishree, Divya, Soubhik, Neha, Pragati, Venkatesh, Thomas, Padmanath, Yuvaraj, Girish, Pethuraj for making my stay at TIFR, a memorable one. Last but not least I would like to thank my family for their constant support throughout my thesis work.

TABLE OF CONTENTS

Page

ACKNOWLEDGMENTS viii

LIST OF FIGURES **xii**

LIST OF TABLES **xv**

SYNOPSIS xvii

BIBLIOGRAPHY **xxix**

Chapters:

1. Introduction **1**

1.1 Bolometer 3

1.2 Ultra Low temperature sensors 4

1.2.1 Semiconductor thermistors 6

1.2.2 Transition edge sensors (TES) 11

1.2.3 Magnetic Micro Calorimeters (MMC) 13

1.2.4 Multiplexed Kinetic Inductance Detectors (MKID) . . . 15

1.3 Neutron Transmutation Doped Germanium (NTD Ge) Sensor . 16

2. Neutron Transmutation Doping of Ge and Radioactive Impurity Studies **20**

2.1 Secondary Ion Mass Spectroscopy 22

2.2 Neutron Irradiation 25

2.3 Radioactive Impurity Measurements 28

2.4 Analysis of Radioactive Impurity Data 34

2.5 Estimation of Φ_{th} from ^{124}Sb 46

2.6 Summary 49

3. Defect studies in NTD Ge **51**

3.1 NTD Ge Surface Studies by SEM-EDAX 54

3.2 Positron Annihilation Lifetime Spectroscopy 56

3.2.1 PALS Experimental Details 56

3.2.2 PALS Results 58

3.3 Channeling 59

3.3.1 Channeling Experimental Setup 61
3.3.2 Channeling Results 63
3.4 Summary 66

4. Characterization of NTD Ge sensors 67
4.1 Fabrication of NTD Ge 67
4.2 Carrier concentration measurement 68
4.2.1 Experimental details 68
4.2.2 Results and discussions 70
4.3 Low temperature measurement 73
4.3.1 4K Cryoinsert for resistivity measurements between 4 to 300 K 74
4.3.2 PID control and development of DAQ 76
4.3.3 Resistance measurement of NTD Ge at mK 80
4.4 Summary 86

5. Summary and Future Outlook 88
5.1 Summary 88
5.2 Future Outlook 93

A. Glossary 95

BIBLIOGRAPHY 97

LIST OF FIGURES

Figure **Page**

1.1 Schematic description of the temperature dependence of the resistivity of a lightly doped semiconductor. 9
1.2 Resolving power of MMC 14
1.3 Working principle of MKID 15
1.4 MIT regime in a range of Ga concentration 18
2.1 Mass spectrum from TOF-SIMS for $< 111 >$ and $< 100 >$ Ge samples. 23
2.2 Ge samples packed for irradiation 26
2.3 Gamma ray spectra of virgin Ge sample compared with ambient background 30
2.4 Gamma ray spectra of n-irradiated Ge sample compared with ambient background 31
2.5 Gamma ray spectra of Ge samples packed in Al foil and in quartz tube 32

2.6 Gamma ray spectra of NTD Ge before and after HF cleaning . 36
2.7 Gamma ray spectra of NTD Ge before and after etching with H_2O_2 37
2.8 Radioactive profile of impurities as a function of etched depth in NTD Ge 38
2.9 Gamma ray spectra of quartz sealed NTD Ge uncleaned, HF cleaned and H_2O_2 etched 39
2.10 Relative neutron fluence estimated from ^{124}Sb activity 48
3.1 Recovery of radiation induced damages as a function of annealing temperature 52
3.2 SEM images of NTD Ge at various stages 55
3.3 Schematic view of PALS set up 57
3.4 Decay scheme of a ^{22}Na nucleus 57
3.5 Typical PALS spectra of Ge 58
3.6 Schematic view of Channeling setup 61
3.7 Samples placed on channeling sample holder. 61
3.8 2D channeling spectra of $< 111 >$ and $< 100 >$ Ge crystal. . . 62
3.9 Axial dip of NTD Ge crystal $< 111 >$ and $< 100 >$ 63
3.10 RBS spectra of Ge sample along $< 111 >$ axis 64
3.11 RBS spectra of Ge sample along $< 100 >$ axis 65
4.1 NTD Ge sample for Hall Effect Measurement 69

4.2 Longitudinal resistance and Transverse voltage of NTD Ge sample at 77 K 69
4.3 Extracted Hall voltage 71
4.4 Comparison of carrier concentration estimated from Hall Effect measurement and from reactor power data 73
4.5 Schematic view of 4K Cryoinsert 75
4.6 4K Cryoinsert setup for resistivity measurements 76
4.7 PID detail 77
4.8 Block diagram of the Labview program with feedback control 78
4.9 Front Panel of the Labview program with feedback control . . 78
4.10 Schematic sketch of the AVS measurement system 79
4.11 Schematic sketch of the NI measurement system 79
4.12 Schematic view of sample mount 81
4.13 Evolution of sample mount for better thermal conductivity . . 81
4.14 Typical signal of resistance measurement 82
4.15 VI characteristics of NTD Ge at 200 mK 83
4.16 VI characteristics of NTD Ge at 10 mK 83
4.17 VI characteristics of NTD Ge at 724 mK 84
4.18 Resistance as a function of temperature for various NTD Ge samples 85
4.19 Linear fit of the logarithmic resistance of NTD Ge with $T^{-0.5}$. 86

LIST OF TABLES

Table **Page**

2.1 Measured isotopic abundances of Ge wafers along with n-capture reaction, stable end products, decay modes and half lives. 24

2.2 Estimated production rate of dopants (atoms/cm^3) per neutron 25

2.3 Details of the irradiated Ge samples 27

2.4 Neutron fluence for different Ge samples 27

2.5 Radionuclides and characteristic γ-rays observed in NTD Ge . 33

2.6 Observed radioactive impurities as a function of the etched depth in NTD Ge sample 41

2.7 Measured radioactivity and estimated cooldown period (T_{cool}) of various NTD Ge sample 42

2.8 Estimated limits on fast neutron induced reaction products in Ge 44

2.9 Estimated traces of ^{123}Sb impurities from the residual radioactivity of ^{124}Sb in the etched NTD Ge samples 47
3.1 Measured positron lifetime (τ_{β^+}) in NTD Ge using PALS. . . 59
3.2 Estimated χ_{min} and N_D of virgin and irradiated samples from the channeling data 66
4.1 Estimated carrier concentration of NTD Ge samples 72

SYNOPSIS

Neutrino is a fundamental particle, which was postulated in 1930 by Pauli [1, 2] to explain beta decay and later in 1934 expounded in the theory of beta decay by Fermi [3]. The neutrino is an electrically neutral Fermion, interacting primarily through the weak force and was initially assumed to be massless. In a path breaking experiment in 1957, Wu et al., [4] showed that beta decay and thus the weak interaction violates parity. The electroweak theory was based on this assumption that neutrinos are massless and only left-handed, along with the complementary right-handed antineutrinos. After a series of observations of neutrino oscillations [5] it was established that neutrinos have a mass, albeit very tiny. The helicity of the massless neutrino is conserved in all inertial frames of reference. However, if the neutrino has a mass then the helicity (or handedness) cannot be a treated as an invariant property. In the meantime, it was hypothesised by Majorana [6] that the neutrino and antineutrino may, in fact, be the same particle. The exact nature of the neutrino, whether it is a Majorana or Dirac, is still unsettled. Hence, the study of neutrinos is important in particle physics for understanding the physics beyond the Standard Model [7].

The mass of the neutrino is an important ingredient to test cosmological and astrophysical theories. There is a concentrated effort to directly determine the neutrino mass using the nuclear beta decay and neutrinoless double beta decay.

In certain nuclei, if the single beta decay (the first order weak interaction) is forbidden due to energy or spin, then such nuclei undergo double beta decay, a second order weak interaction. However, if the neutrino is a Majorana particle, in the case of nuclei undergoing double beta decay, there is a possibility of annihilations of the two neutrinos leading to a neutrinoless double beta decay (NDBD) process. The experimental observation of NDBD would imply the neutrino to be a Majorana particle and can pave a way to the physics beyond the standard model.

There are several experiments for the search of Majorana nature of the neutrino [8]. In India, efforts have been recently taken to search for NDBD in ^{124}Sn. The INdia-based TIN (TIN.TIN) detector [9] will be housed at the upcoming India based Neutrino Observatory (INO). This experiment involves the development of cryogenics bolometer detector operating at a milli-kelvin temperature to look for the thermal pulses corresponding to $Q_{\beta\beta}$ value of ^{124}Sn, which is 2292.64 ± 0.39 keV [10]. In order to measure

the temperature rise of the detector ($\sim$ 100 μK) with a high precision, sensors with low specific heat, fast rise time and high temperature sensitivity are needed.

Several sensors [11] possess one or the other of the above mentioned properties. The most commonly used cryogenic sensors are Neutron Transmutation Doped (NTD) Ge sensor, Transition Edge Sensor (TES), Magnetic microcalorimeters (MMC)and Multiplexed Kinetic Inductance Detectors(MKID). NTD Ge sensor is highly preferred for mass production, reproducibility and simpler readout. This semiconductor thermistor also possesses high temperature sensitivity which is the most crucial requirement for a bolometric detector. Hence for the TIN.TIN bolometer NTD Ge sensor is chosen as the thermal sensor.

Neutron Transmutation Doped (NTD) Ge sensor has been widely used as low temperature sensors in mK range for bolometric detectors in dark matter search [12] and neutrino physics [13]. The NTD Ge sensor has good uniformity of dopants compared to the conventional melt doped Ge samples. The conduction mechanism of the NTD Ge sensors at low temperature is believed to be in Variable range Hopping(VRH) mechanism [14]. It has been reported [15] that doping Ge samples close to the metal-insulator transition produces thermistors with low noise, high temperature sensitivity and

excellent reproducibility at an ultra low temperature. The temperature dependence of the resistivity of a NTD Ge sensor is given by [16],

$$\rho = \rho_0 \, exp(T_0/T)^{\alpha} \tag{1}$$

where the α is predicted to be 0.5, in a VRH. The value of ρ_0 and T_0 can be tuned by the neutron fluence.

The NTD Ge samples were prepared by irradiating Ge wafers with thermal neutrons in a reactor. The natural Germanium consists of five isotopes. During irradiation, all the five isotopes undergo neutron capture. The isotopes specifically, ^{70}Ge, ^{74}Ge and ^{76}Ge capture a neutron and transmute into dopants such as ^{71}Ga, ^{75}As and ^{77}Se, respectively. For natural Ge, due to the isotopic abundances and thermal neutron capture cross sections, the irradiated Ge wafers result in a p-type semiconductor arising due to the dominant impurity, ^{71}Ga.

The net charge carriers formed, given by $N_A - N_D$ (carrier density due to acceptor - donor impurities), is related to the concentrations of the impurities $[N_{^{71}Ga} - (N_{^{75}As} + 2 \times N_{^{77}Se})]$. Fabricating NTD Ge sensors involves step-wise process such as neutron irradiation of Ge wafers, study of radioactive impurities formed due to neutron irradiation, study of fast neutron induced damages, verifying and optimizing the dopant concentration, preparing resistance thermometers and characterising it at mK temperature.

This thesis will describe the experimental techniques and the measurements to understand these processes, towards the indigenous development of the NTD Ge sensors for the TIN.TIN experiment.

Neutron Transmutation Doping of Germanium:

Neutron Irradiation:

Semiconductor grade Ge wafers are irradiated with thermal neutrons from the 100 MW Dhruva research reactor [17] at Bhabha Atomic Research Centre, Mumbai. The Ge samples wrapped in Aluminium were irradiated at designated ports. The Ge wafers with cleavage planes of $< 111 >$ (0.4 mm thick, $\rho \sim 30\ \Omega$ cm) and $< 100 >$ (1 mm thick, $\rho \sim 35\ \Omega$ cm) were used for producing NTD Ge sensors. Prior to irradiation, samples were cleaned in an ultrasonic bath with electronic grade isopropyl alcohol for about 15 min and blow dried with dry N_2. Samples were loaded in a specially designed capsule as per the mandatory procedure for irradiation in the Dhruva reactor. Different mounting arrangements permissible within operational constraints of the irradiation protocols in the reactor were tried out to assess the effect of wrapping material and irradiation environment. These consisted of a single sample wrapped in Aluminium foil, three stacked samples wrapped in a common Aluminium foil and three stacked samples inside a quartz tube.

Radioactive Impurity studies:

During neutron irradiation, the exposure to high neutron dose can also lead to radioactive contamination of Ge sensors due to various causes [18] arising from handling, surface contamination, etc., even if the starting material is of high purity. Trace radioactivity in sensors can produce significant background for rare event studies like double beta decay. Moreover, the radioactive contaminants can also act as a heat load when the sensors are used in mK temperature. In order to study the radioactive contaminates, spectroscopic investigations were carried out on the neutron irradiated Ge samples using low background Higher Purity Ge (HPGe 70 % efficient) detector [19, 20]. In the studies the irradiated samples showed several radioactive isotopes such as ^{110m}Ag, ^{124}Sb, ^{184}Ta, etc. Chemical etching methods were tried on NTD Ge samples in order to know whether the radioactive impurities are on the surface or in the bulk. It was found that most of the impurities were surface contaminants and only ^{124}Sb remains in $< 100 >$ and ^{110m}Ag remains in $< 111 >$ NTD Ge, even after etching 50 μm of Ge layer from the samples. Hence, the parent of these radioactive impurities namely ^{123}Sb and ^{109}Ag, were considered to be a bulk impurity and were estimated to be present in the ppt level in the parent Ge wafers. The measured level of ^{124}Sb was also used as a cross check to correlate the neutron

fluence obtained from the reactor power. If the etched samples were allowed to cool down for a period of 2 yrs after irradiation, the activity can fall below 1 mBq/g. To reduce activity from residual surface contamination, pre-etching of samples prior to n-irradiation will be highly desirable. The chemical etching does not affect the performance of the sensor but is desirable even from thermometry consideration since radioactive impurities can produce a significant background and can act as a standing heat load at mK temperature. For the desired neutron fluence of 1 - 5 x 10^{18} /cm^2, removal of 50 μm surface layer is found to be adequate for this purpose. The studies on radioactive impurities in NTD Ge is described in this thesis and is reported in Ref. [20].

Defects studies:

The dopants in the NTD Ge samples are formed mainly due to thermal neutrons. But the reactor neutrons are not monoenergetic and the fast neutrons can create defects in the crystal lattice structure. These defects can affect the carrier concentration formed in the samples [21]. Hence, it is necessary to study the neutron induced damages in the NTD Ge samples. Two different techniques namely Positron Annihilation Lifetime Spectroscopy (PALS) and low energy α-Channeling were employed to study the defects in NTD Ge samples. The PALS was done at BARC, Mumbai. In this method, the lifetime of the positron in the NTD Ge samples were measured.

The PALS showed that most of the neutron irradiated sample has defects of monovacancy type. Due to the saturation in the measured lifetime of positron corresponding to the monovacancy, the defect density cannot be quantified and has been estimated to be greater than 0.1 %.

The Channeling experiment has been carried out with a 2 MeV alpha beam at PARAS facility, IUAC, New Delhi. This Channeling technique showed that there were no significant defects for the samples exposed to the fast neutron fluence of less than 4 x 10^{16}n/cm^2. The defect densities of the samples irradiated with higher neutron dose were estimated to be $\sim$ 7 x 10^{20}/cm^3. Both the techniques confirmed that the defects get fully cured by annealing the NTD Ge samples at 600 ^{o}C for 2 hrs in a vacuum sealed quartz capsule. This was standardized as the annealing procedure and has been followed to make the irradiated Ge samples defect free. The details of defect studies [22] on NTD Ge are presented in this thesis.

Characterizing NTD Ge sensors:

Fabrication of NTD Ge sensors:

The irradiated Ge wafers were cleaned with HF in order to remove the surface oxide layers. Then the samples were annealed at 600 ^{o}C for 2 hours in a vacuum sealed quartz tube, to cure the lattice defects induced by the fast neutrons. The radioactive contaminants on NTD Ge samples were removed by etching about 50 μm of Ge layer, by treating with H_2O_2 at 80 ^{o}C. This

procedure ensured that the samples were free from defects and from the radioactive contaminants.

For characterizing the sensors, a pattern of ohmic contacts were made on the etched and cleaned NTD Ge samples. For Hall measurement, the contact pad were in Van de paw [23] pattern (pattern of six pads) and for resistivity measurement it was two pads on the surface of the samples. This was a critical process and depended crucially on the choice the contact material, as it has to make ohmic contact as well as withstand the thermal cycles from room temperature to mK temperature. Initially various elements like In, Al were tried on Ge samples and finally the optimal contact pads were made by depositing Au-Ge alloy by sputtering technique. The contact pads were standardized and prepared by depositing Au(88%) - Ge(12%) of about 50 nm thickness and rapid thermally annealing at 400° C for 2 min in dry N_2 atmosphere. The Au-Ge contact pads on the NTD Ge sample were wedge bonded with Aluminum wires (ϕ = 25 μm) to the Au pads on the mounting chip, for making the electrical connections. These contacts were also demonstrated to be resilient to repeated thermal cycling.

Hall Effect measurement:

The NTD Ge samples has to be irradiated with the optimum neutron fluence in order to tune the sensors to work at the mK range. The Secondary Ion Mass Spectrometry was used to measure the isotopic abundance of the

Ge wafers. The carrier concentration can then be estimated with the neutron fluence obtained from the reactor power. The carrier concentration was also estimated experimentally by Hall Effect measurement at TIFR. The Hall voltage was measured at 77 K and 300 K by varying magnetic field between -1 to 1 tesla. The carrier concentrations were then estimated from the measured Hall voltages. The carrier concentration estimated at 77 K agree with that of calculated carrier concentration with the neutron fluence [22]. However, carrier concentrations estimated at 300 K were higher than the actual carriers. As explained by Morin [24], at 77 K the Hall factor was close to unity, whereas at 300 K it was $\sim$1.8. In the NTD Ge samples the Hall factor at 77 K was similar to the value quoted by Morin, whereas it varied between 1.2 to 1.9 at 300 K. The carrier concentration estimated at 77 K was also used to verify the neutron fluence obtained from the reactor power.

Low Temperature Measurement :

The NTD Ge sensors were then characterized at mK temperature with a custom built cryogen free dilution refrigerator, CFDR-1200 [25]. The Labview acquisition program has been developed to acquire the data using AVS resistance bridge as a part of this thesis work. The samples with six contact pads and smaller size samples with two contact pads were used in resistance measurements. Sensors with various neutron fluence were also tested. Samples irradiated with neutron fluence of the order of 10^{19}/cm^2

showed metallic behaviour which makes it unsuitable to use it as sensors at low temperature. The annealed samples with carrier concentration in the range 0.5 - 1 x $10^{17}/cm^3$ are found to be suitable for the sensors developed to be operated below 100 mK. These lower neutron dose samples showed good sensitivity and reproducibility at mK temperature. Moreover, these sensors follow the Mott′s variable range hopping model (Eqn. 1.11), with α around 0.5, from 75 mK - 250 mK. The sensor prepared from the NTD Ge sample has shown very promising results in the temperature range 75 to 250 mK, with large dR/dT $\sim$ 2.3 kΩ/mK at 100 mK.

In summary, this thesis describes the fabrication and characterization of NTD Ge sensors developed for the first time in the country. In the first chapter of the thesis, the significance of neutrinoless double beta decay in understanding the nature of the neutrino is briefly introduced and the necessity of the high sensitivity temperature sensors for a bolometric experiment is described. The chapter also gives a brief introduction to semiconductor thermistor, Neutron Transmutation Doped Germanium (NTD Ge) sensors. The second chapter describes the method of Ge sample preparation for neutron irradiation and the radioactive impurity study in NTD Ge sensors with low background HPGe detector. The third chapter describes the study of fast neutron induced damages on NTD Ge by PALS and Channeling technique and the annealing procedure used for curing defects. The fourth chapter

presents the studies carried out for characterizing Neutron Transmutation Doped Ge sensors. This chapter elaborates the fabrication procedure of NTD Ge sensor, followed by the Hall effect measurement and resistivity measurement at low temperature using the top loading probe in the dilution refrigerator. This chapter also describes the construction of a 4K resistivity measurement setup and the details of data acquisition programming with Labview. Summary and future outlook are presented in Chapter five.

BIBLIOGRAPHY

[1] References to early literature on the subject can be obtained in K Winter (ed): Neutrino Physics (Cambridge University Press 1991).

[2] For an English translation of the text of this letter, see Pauli's article in Ref.[1].

[3] E. Fermi: Ricercha Scient. **2** (1933); ZPh **88** (1934) 161.

[4] C. S. Wu et al., Physical Review, **105** (1957) 1413.

[5] K. Nakamura and S. T. Petcov, Neutrino Masses, Mixing and Oscillations in J. Beringer et al. (Particle Data Group), Phys. Rev., D **86** (2012) 010001.

[6] E. Majorana, Nuovo Cimento **5** (1937) 171.

[7] R.N. Mohapatra and P.B. Pal, Massive neutrinos in physics and astrophysics. Second edition, World Sci. Lect. Notes Phys. **60** (1998) 1.

[8] A. Barabash, arXiv:1403.2870.

[9] V. Nanal, EPJ Web of Conferences **66** (2014) 08005.

[10] D.A. Nesterenko et al., Physical Review C, **86** 044313 (2012).

[11] Cryogenic Particle Detection, Topics Appl. Phys. **99** (2005), Chr. Enss (Ed.), Springer-Verlag Berlin Heidelberg.

[12] O. Martineau et al., Nuclear Instruments and Methods in Physics Research Section A, **530** (2004) 426.

[13] C. Arnaboldi et al., (CUORE Collaboration), Nuclear Instruments and Methods in Physics Research Section A, **518** (2004) 775.

[14] D. McCammon, Cryogenic Particle Detection, Topics Appl. Phys. **99** (2005) 35.

[15] A.L. Woodcraft et al., Journal of Low Temperature Physics **134** (2004) 925.

[16] P.L. Richards, Journal of Applied Physics, **76** (1994) 1.

[17] S.K. Agarwal et al., Nuclear Engineering and design, **236** (2006) 747.

[18] A. Alessandrello et al., Nuclear Instruments and Methods in Physics Research Section B **93** (1994) 322.

[19] N. Dokania et al., Nuclear Instruments and Methods in Physics Research Section A , **745** (2014) 119.

[20] S. Mathimalar et. al., Nuclear Instruments and Methods in Physics Research Section A , **774** (2015) 68.

[21] R.R. Hasiguti, Defects and Radiations Effects in Semiconductors, (1980) 46.

[22] S. Mathimalar et. al., Nuclear Instruments and Methods in Physics Research Section B, **345** (2015) 33.

[23] L.J. Van der Pauw, Phil. Res. Rep. **13** (1958) 1.

[24] F.J. Morin, Physical Review **93** (1954) 62 .

[25] V. Singh et. al., Pramana - Journal of Physics **81** (2013) 719 .

[26] S. Mathimalar et. al., IEEE WOLTE conference (2014)
doi: 10.1109/WOLTE.2014.6881014.

Chapter 1

Introduction

Neutrino is a fundamental particle and was postulated in 1930 by Pauli [1, 2] to explain beta decay. The neutrino is an electrically neutral Fermion, interacting primarily through the weak force and was initially assumed to be massless. Reines and Cowan [3] experimentally discovered the neutrino by observing the inverse beta decay from the reactor antineutrino. In a path breaking experiment in 1957 Wu et al. [4] showed that the beta decay and thus the weak interaction violates parity. Subsequent neutrino oscillation experiments showed the neutrinos have a very tiny mass [5]. In certain nuclei if the single beta decay (the first order weak interaction) is forbidden due to energy or spin, then double beta decay (DBD) - a second order weak interaction can occur. If the neutrino is a massive Majorana particle there is a possibility of virtual annihilation of the two neutrinos in DBD leading to a neutrinoless double beta decay($0\nu\beta\beta$) process. Two neutrino double

beta decay process ($2\nu\beta\beta$) was suggested first by M. Goeppert Mayer in 1935 [6] and it can be expressed as,

$$N(A,Z) \rightarrow N(A,Z+2) + 2e^- + 2\bar{\nu}_e \quad (2\nu\beta^-\beta^-) \tag{1.1}$$

$$N(A,Z) \rightarrow N(A,Z-2) + 2e^+ + 2\nu_e \quad (2\nu\beta^+\beta^+) \tag{1.2}$$

The $0\nu\beta\beta$ decay was proposed four years later by W. H. Furry [7] and is represented as,

$$N(A,Z) \rightarrow N(A,Z+2) + 2e^- \quad (0\nu\beta^-\beta^-) \tag{1.3}$$

$$N(A,Z) \rightarrow N(A,Z-2) + 2e^+ \quad (0\nu\beta^+\beta^+) \tag{1.4}$$

About 35 nuclei [8] have been predicted to undergo double beta decay and a similar number of nuclei are predicted to decay by double positron decay. The experimental observation of $0\nu\beta\beta$ would confirm the Majorana nature of Neutrino and can pave a way to physics beyond the standard model. It should be noted that $0\nu\beta\beta$ violates the total lepton number conservation. At present, the search for $0\nu\beta\beta$ is the only possible experiment to probe the Majorana nature of neutrinos. The experimental signature of $0\nu\beta\beta$ decay is the constancy of sum energy of two electrons equal to Q value of the reaction. There are many experiments worldwide searching for $0\nu\beta\beta$ [9]. In India, efforts have been recently initiated to search for $0\nu\beta\beta$

in ^{124}Sn. The INdia based TIN (TIN.TIN) detector [10] will be housed at the upcoming India based Neutrino Observatory (INO). This experiment involves the development of cryogenic bolometer detector operating at millikelvin temperature to look for the thermal pulses corresponding to $Q_{\beta\beta}$ value of ^{124}Sn, which is 2292.64 $\pm$ 0.39 keV [11]. In order to measure the temperature rise of the detector ($\sim$ 100 μK) with a high precision, sensors with low specific heat, fast rise time and high temperature sensitivity are needed. Neutron Transmutation Doped (NTD) Ge sensor is an optimum sensor to employ at mK temperature. This thesis is focused on the indigenous development of NTD Ge sensor in the country, by irradiating Ge wafers in the Dhruva reactor [12] at Bhabha Atomic Research Centre (BARC), India.

1.1 Bolometer

First bolometer or actinic balance (thermic balance), working at room temperature was invented by S. P. Langley for infrared astronomy [13, 14]. The design consisted of two metal strips which formed the virtual arms of the Wheatstone's bridge. One of the metal strips was exposed to the radiation and change in its resistance was measured. Later the bolometer design concept was modified to include an absorber and a thermal sensor. Bolometers operating at mK can yield high energy resolution. The absorber in the

bolometer can be either a superconductor or an insulator, as the specific heat is very low for these materials in the millikelvin temperature range. The thermal sensor has to be highly sensitive and accurate for obtaining good energy resolution. NTD Ge is a promising sensor technology which has been widely used in space and infrared astronomy applications [15, 16]. It has made its presence felt in the experiments searching for rare decay events as well. Some of these experiments run at mK temperature obtained by Cryogen free dilution refrigerator (CFDR) [17].

1.2 Ultra Low temperature sensors

For a high energy resolution bolometric experiment, the performance of the sensor matters significantly. As mentioned earlier, initial thermal detectors used a metal for measuring the radiation. After the discovery of superconductivity by H.K. Onnes in metallic Hg [18], in the year 1911, the superconductor was available for the experimentalist for making sensitive thermometers. In the superconducting state, the resistance of the metal vanishes abruptly. Superconducting thin films were tested as resistance thermometers in 1938 for the measurement of a small quantity of energy [19]. Andrews *et.al.*, in 1941 had used a receiver (absorber) made out of Pb thin film on a glass plate, for measuring Infrared radiation [20]. They had kept the receiver at 7 K which is the transition temperature (T_c) of Pb, below

which Pb is superconducting and above which it behaves as a normal metal. In the following year, Andrews *et.al.*, had used a Ta filament [21] as the thermometer cemented on an Aluminum absorber operated at 4 K. In the modified design of the bolometer, the energy incident on the absorber is reflected by a sharp change in the resistance of the thermometer. The measured ratio of the potential drop to the incident energy was about a several order of magnitude higher than the normal method of radiation detection. This drastically increased the thermometric sensitivity of the detector. The device was named as a "superconducting bolometer" [21] since it had used a superconducting thermistor.

Following the superconducting thermistor, Boyle and Rogers [22] had used Carbon resistor, both as an absorber as well the resistance thermometer. The advantage of carbon sensor is its low cost and easy fabrication. The prime advantage of the carbon material is its reduced specific heat at low temperature. The main drawback of the carbon material is that it comes with excess low frequency noise which limits the sensitivity of the bolometer. Moreover, the reproducibility of the carbon sensors was also inconsistent. Low [23] had showed lightly doped Ge crystal, using neutron transmutation technique can provide a highly preferable bolometric sensor. In this technique compensated carriers take part in the conduction mechanism. The details of the Neutron Transmutation Doped Ge are given in section 1.3.

Recently, a lot of new technologies have been developed which can substitute the conventional bolometric sensors. Few of them are Transition edge sensor (TES), Magnetic Micro Calorimeters (MMC) and Multiplexed Kinetic Inductance Detectors (MKID). A brief discussion about the working principle and the merits of these sensors are provided in the following sections.

1.2.1 Semiconductor thermistors

At very low temperature thermocouples and metallic thermistors do not possess enough sensitivity to detect the temperature change. Pure semiconductors were used at a higher temperature, but at low temperature the resistance becomes too large, thus making the measurement difficult. Hence, these semiconductors need to be doped to a certain level to make the resistance measurable and ensuring good sensitivity to detect the temperature change.

Intrinsic carriers play a significant role in the conductivity of the semiconductor at higher temperature due to thermal activation energy and the temperature dependency of these intrinsic carriers concentration are given by the following equation.

$$n = p = \frac{(2\pi\sqrt{m_e m_h} kT)^{3/2}}{4\pi^3\hbar^3} \, exp(-E_g/2kT) \tag{1.5}$$

where m_e and m_h are the masses of electrons and holes, respectively. E_g represents the forbidden energy gap.

In case of extrinsic carriers the results depends on the relation between the number of empty positions KN_D due to compensation and the number of empty positions n(T) due to the thermal excitation of carriers into the conduction band. For $KN_D << n(T)$ the Fermi level is located midway between donor level and the bottom of the conduction band, thus

$$n(T) = [N_D N_C/2]^{1/2} \, e^{-E_0/2kT} \tag{1.6}$$

where

N_A - acceptor concentration

N_D - Donor concentration and

$$N_C = \frac{(2\pi m_e kT)^{3/2}}{4\pi^3 \hbar^3} \tag{1.7}$$

For $n(T) << KN_D$ the Fermi level is close to the isolated donor level, and given as:

$$n(T) = [N_C(N_D - N_A)/2N_A] \, e^{-E_0/kT} \tag{1.8}$$

In an undoped semiconductor, the resistance of the material increases as temperature decreases. In case of a lightly doped semiconductor, the resistance initially decreases and further lowering of temperature increases

the resistance. For a heavily doped semiconductor, the resistivity follows the metallic nature.

Figure 1.1 shows a schematic plot (semilog ρ vs T^{-1}) of lightly doped semiconductor. The intrinsic carrier conduction is shown in the region A, whereas the conduction due to extrinsic carriers is shown in the regions B-D. The regime B is called the saturation range, where the impurities are ionized and hence carrier concentration is independent of temperature. In this regime, the conduction is purely due to the mobility of the carriers. Further lowering of temperature leads to freezing out of the impurity carriers (temperature range C). Below a certain temperature, the electrical conductivity is mainly contributed by the electrons hopping directly from one to another impurity atom without reaching the conduction band. This particular conductivity is called hopping conductivity and is represented as region D in Figure 1.1. In hopping mechanism, conductivity is due to very low mobility since carriers wave function weakly overlap with the nearby impurity atoms. In case of Ge crystal doped with a carrier concentration of $\sim 10^{15}/\mathrm{cm}^{-3}$, the regime A corresponds to $T > 400$ K, range B varies from $50\ \mathrm{K} < T < 400\ \mathrm{K}$, range C corresponds to $7\ \mathrm{K} < T < 50\ \mathrm{K}$ and the hopping mechanism regime D occurs at 7 K.

The hopping mechanism was theoretically predicted by Gudden and Schottky [25] and later experimentally observed by Bush and Labhart [26] in SiC

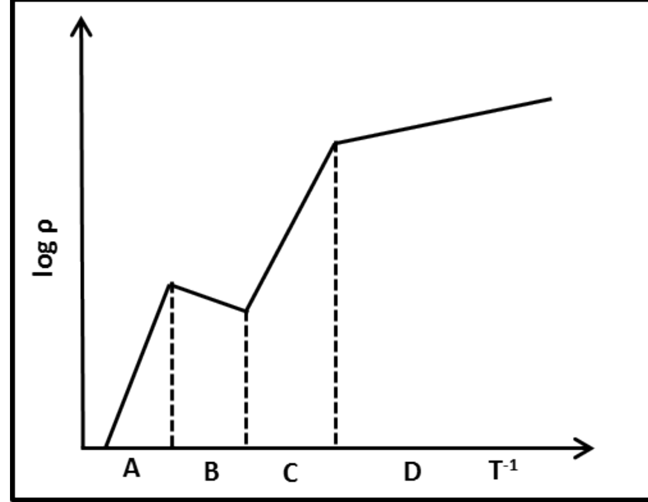

Figure 1.1: A schematic description of the temperature dependence of the resistivity of a lightly doped semiconductor. The conduction mechanism in the labeled regions can be identified as follows: (A) Intrinsic conduction (B) Saturation of impurity conduction (C) Freeze out and (D) hopping conduction. Figure from [24].

and by Hung and Gliessman [27] in Ge and Si for the first time. In order to produce thermometers that can operate in the range around 10 mK which lies in the VRH regime, the dopant level needs to be optimized.

Mott had formulated the probability (P_{ij}) of a carrier tunneling from a localized state i with energy E_i to a empty state j with energy E_j as

$$P_{ij} = exp(-2aR_{ij} - (E_j - E_i)/K_B T) \qquad if \;\; E_j > E_i \tag{1.9}$$

$$P_{ij} = exp(-2aR_{ij}) \qquad if \;\; E_j \leq E_i \tag{1.10}$$

where a is a parameter related to the barrier tunneling.

The hopping probability at higher temperature is dominated by spatial coordinates and it is known as nearest neighbor hopping mechanism. However at sufficiently low temperature the hopping takes place to the energetically favored site rather than spatially near site. This hopping mechanism is called as VRH and the variation of resistivity with respect to temperature in this regime is given by the following equation.

$$\rho = \rho_0 \, exp(T_0/T)^{\alpha} \tag{1.11}$$

In the case of NTD Ge sensor where the doping is carried out by neutron transmutation, the value of ρ_0 and T_0 (characteristic temperature) can be tuned by the neutron fluence. According to Mott's theory, the variable R_{ij} and E_{ij} describes the hopping probablity in four dimensions leads to α as 1/4. Efros and Shklovskii [28] later showed that the VRH regime is described more appropriately with a value of α equal to 1/2. The conventionally doped Si and Ge do not follow this equation. However, Ge wafers doped by neutron transmutation method [29] and the Si thermistors produced by ion implantation method [30] show this behaviour. Both the crystals can be used as sensitive resistance thermometer at very low temperature. The choice of using either Ge or Si strongly depends on the application. Neutron Transmutation doped Ge (NTD Ge) is best for its excellent reproducibility, whereas ion implanted Si is easy to fabricate.

NTD Ge

As mentioned earlier, NTD Ge sensors are produced by doping Ge wafers by neutron transmutation technique. In this technique, the Ge wafers are irradiated with thermal neutrons from a nuclear reactor and the wafer gets uniformly doped. The conventional melt growth method does not provide the necessary uniformity in the doping. The complete description of NTD Ge is given in section 1.3

Ion implanted Silicon

For neutron transmutation method, Si needs a higher level of neutron dose to get doped to the necessary level. The semiconductor industry has optimized the doping method by ion implantation from a beam of kinetic energy of from keV to few MeV. The doping can be achieved up to the depth of 1 μm by ion implantation. In this method, the dopants get a gaussian density depth profile. The main advantage of this sensor is that it can be produced in large numbers simultaneously using photolithography masking technique.

1.2.2 Transition edge sensors (TES)

Transition Edge Sensor (TES) is a superconducting thin film, operated just below its transition temperature (T_C). The energy deposition can drive

the superconducting TES to a normal state, hence a sharp change in resistance can be sensed in TES even for a small change in temperature. The figure of merit of this resistance thermometer is given by its logarithmic temperature sensitivity (α).

$$\alpha = \frac{T}{R}\frac{dR}{dT} \tag{1.12}$$

The TES can be two orders of magnitude more sensitive than the semiconductor thermistors. A.E Lita et.al., [31] had successfully tuned the T_C of W thin film around 100 mK by merging the α and β phase of W. The deposition condition plays a vital role in the microscopic structure of W. Hence the authors came up with a model, which can provide the necessary T_C depending on the deposition condition such as deposition power and Ar pressure in the deposition chamber. T.C. Chen et.al., [32] had used the proximity effect of Mo/Au bilayer to tune the T_C of the TES in the range of 50 - 600 mK. They could produce TES sensor with logarithmic sensitivity(α) as high as 2500. Many bolometric experiments in astronomy and rare decay studies uses TES for its high sensitivity, irrespective of its complicated SQUID readout system.

1.2.3 Magnetic Micro Calorimeters (MMC)

Dependence of magnetization of paramagnetic salt with a change in temperature is the principle used in Magnetic Micro Calorimeter (MMC). The low temperature MMC is presumed to be mentioned for the first time in a diploma thesis [33] of W. Seidel of the Technical University in Munich in 1986. Efforts have been taken at Walther Meissner Institute in Munich for producing MMC and Umlauf et al [34] had demonstrated the use of magnetization of 4f ions in a dielectric absorber to measure small energy inputs. But the response time was slower at low temperature due to the weak coupling of the magnetic moment to the phonons. Later it was suggested that the absorber material can be changed from dielectric to metallic absorber [35]. Relaxation time of the paramagnetic ion in the metallic medium is faster than in the dielectric medium and thus it reduce the response time of such thermometer by several orders of magnitude. But the faster response time was obtained at the expense of an increase in specific heat due to the conduction electrons. In spite of the higher specific heat, MMC has excellent resolving power compared to that of other microcalorimeters.

For a given MMC, the change in magnetization due to incident radiant energy δE is given by,

$$\delta M = \frac{\partial M}{\partial T}\delta T = \frac{\partial M}{\partial T}\frac{\delta E}{C_{tot}} \tag{1.13}$$

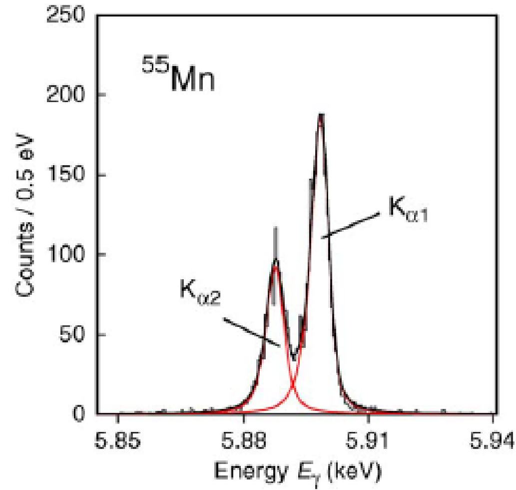

Figure 1.2: K_α spectrum of ^{55}Mn in a MMC detector. The solid line represents a fit of the data taking into account the natural linewidth as determined with a crystal spectrometer. Figure from [36].

where δT is the change in temperature of the calorimeter with a heat capacity (C_{tol}) of both thermistor and absorber.

A. Fleischmann et.al., had made a prototype of X-ray detector with the Au-Er sensor attached to an Au absorber. They could obtain an excellent energy resolution of 3.4 eV at 6.5 keV [36]. Figure 1.2 shows the well resolved K_α spectrum of ^{55}Mn in a MMC detector [36].

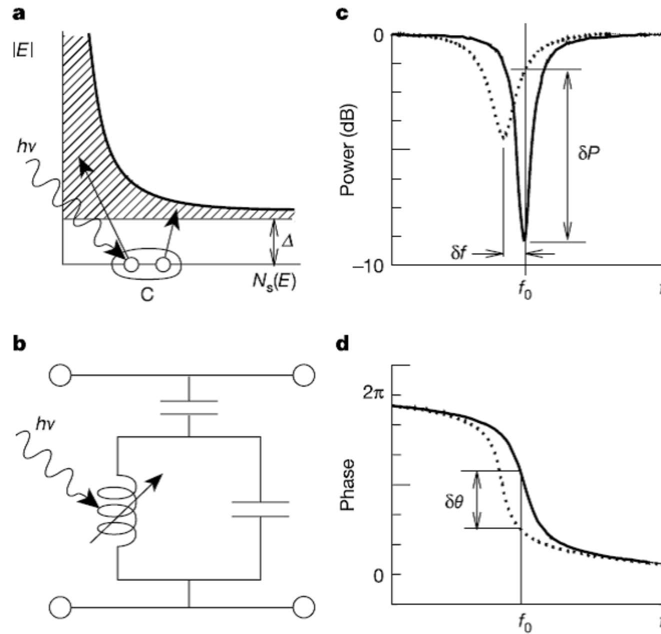

Figure 1.3: Working principle of MKID. (a) Energy (hν) incident on superconducting film, produces the quasi particle (b) Change in quasi particle density changes surface impedance (c) and (d) show the typical amplitude and phase response of a microwave excitation signal. Figure from [37].

1.2.4 Multiplexed Kinetic Inductance Detectors (MKID)

The basic working principle of MKIDs is the change in surface impedance of a superconducting film for an incident photon energy, through kinetic inductance effect. The incident energy breaks the cooper pairs in the superconducting film and produces the quasi particles. The excess quasi particle changes the surface impedance of the superconducting film. The above mentioned processes are depicted in Figure 1.3.

Generally, the coil is deposited on the superconducting film, with an insulating layer in between. The detector is matched with the SQUID amplifier. MKIDs allow to multiplex up to 10^3 - 10^4 read out channels on a single coaxial cable. Thus, this reduces the required number of wirings and preamplifier to a considerable amount which needs to be taken care in large array detectors. Hence, MKIDs might be a preferable sensor for the future experiments.

1.3 Neutron Transmutation Doped Germanium (NTD Ge) Sensor

NTD Ge is widely used in bolometric detectors for excellent reproducibility. Natural Ge possess following five isotopes, ^{70}Ge, ^{72}Ge, ^{73}Ge, ^{74}Ge and ^{76}Ge. Neutron irradiation on these Ge isotopes undergo the (n, γ) reaction (refer equations 1.14 to 1.18), when there is a single neutron capture.

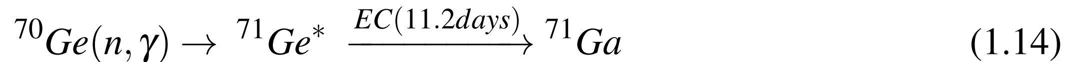

$$^{70}Ge(n,\gamma) \rightarrow \ ^{71}Ge^* \xrightarrow{EC(11.2days)} \ ^{71}Ga \tag{1.14}$$

$$^{72}Ge(n,\gamma) \rightarrow \ ^{73}Ge \tag{1.15}$$

$$^{73}Ge(n,\gamma) \rightarrow \ ^{74}Ge \tag{1.16}$$

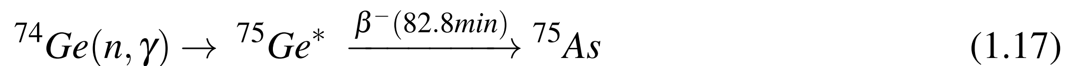

$$^{74}Ge(n,\gamma) \rightarrow \ ^{75}Ge^* \xrightarrow{\beta^-(82.8min)} \ ^{75}As \tag{1.17}$$

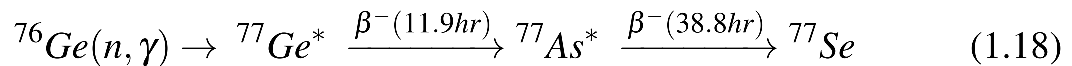

$$^{76}Ge(n,\gamma) \rightarrow \ ^{77}Ge^* \xrightarrow{\beta^-(11.9hr)} \ ^{77}As^* \xrightarrow{\beta^-(38.8hr)} \ ^{77}Se \tag{1.18}$$

Among the above reaction products, ^{73}Ge and ^{74}Ge are stable and hence do not contribute in the carrier concentration. The products ^{71}Ga contribute holes whereas ^{75}As and ^{77}Se contribute electrons. Natural isotopic abundance and the neutron capture cross section results in a ^{71}Ga rich irradiated Ge sample. and thus making it a p-type semiconductor. The net charge carriers formed is given by $\mathrm{N_A - N_D}$ (difference of acceptor and donor charge density) and is related to the concentrations of the impurities by the following equation,

$$\mathrm{N_A - N_D} = [\mathrm{N}_{^{71}\mathrm{Ga}} - (\mathrm{N}_{^{75}\mathrm{As}} + 2 \times \mathrm{N}_{^{77}\mathrm{Se}})] \tag{1.19}$$

Compensation ratio K is given by the ratio of minority to majority carriers. The CUORE, a bolometric experiment at Gran Sasso for search of neutrinoless double beta decay, characterized the NTD Ge sensor with the carrier concentration in the range (5.0 - 6.8) $\times 10^{16}/cm^3$ and found 6.8 $\times 10^{16}/cm^3$ to be the best choice for their detector [38]. K.M. Itoh et.al., [29] measured the hopping conductivity of natural Ge with a carrier concentration of (0.03 - 8.6) $\times 10^{16}/cm^3$ and with the compensation ratio of 0.32. The authors have compared the conductivity of natural Ge with the ^{70}Ge enriched wafer, with carrier concentration of (3 - 18) $\times 10^{16}/cm^3$ and the compensation ratio of

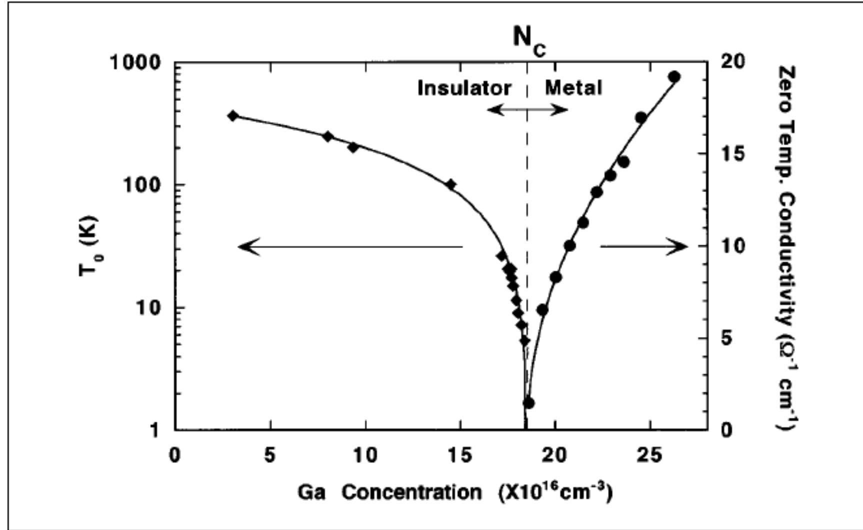

Figure 1.4: Extrapolated zero temperature electrical conductivity (right axis) and characteristic temperature T_0 (left axis) determined from the experiment, as a function of Ga concentration. The MIT regime is found to occur at an acceptor concentration of $18.6 \times 10^{16}/cm^3$. Figure from [39].

< 0.001. Both the NTD Ge sensors behaved differently in the hopping conductivity and moreover for the temperature above 300 mK, enriched Ge was found to possess factor of two higher sensitivity than the natural Ge.

Figure 1.4 shows an experimental plot [39] of the conductivity of NTD Ge for a range of Ga concentration at a various characteristic temperature (T_0). In this particular experimental results, the transition from insulator to metal occurs in Ge for a Ga concentration of about $18 \times 10^{16}/cm^3$. This transition regime is widely known as Metal Insulator Transition (MIT). To obtain a high sensitivity thermometer, the Ga concentration preferred to be just below this MIT regime.

A program to develop low temperature (mK) sensors with NTD Ge for neutrinoless double beta decay studies with cryogenic bolometer has been initiated. Presently a prototype bolometer with superconducting Tin absorber is under development [10], which will be later housed at the upcoming underground laboratory INO [40].

This thesis describes the indigenous development of NTD Ge sensor in the following chapters. The fabrication of NTD Ge sensors and characterization studies together with the development of instrumentation for mK thermometry are presented.

Chapter 2

Neutron Transmutation Doping of Ge and Radioactive Impurity Studies

The NTD Ge thermistors have been widely used as low temperature sensors (in mK range) for bolometric detectors in dark matter searches and neutrino physics [41, 42]. Compared to the conventional metallurgical methods, neutron transmutation doping yields good uniformity and is found to show good reproducibility [43, 44]. Highly sensitive NTD Ge sensors can be fabricated by doping Ge wafers just below the MIT regime. Hence, the neutron fluence for Ge doping needs to be optimized depending on the isotopic abundance of Ge sample. Further, during irradiation the exposure to high neutron dose can lead to radioactive contamination of Ge sensors [45] due to surface impurities and other sources, even if starting material is of high purity (5N). Such trace radioactivity in sensors can produce significant background for rare event studies like double beta decay. It is, therefore, important to study

and minimize the production of relatively long lived impurities in NTD Ge prior to sensor development. A significant cooldown period for sensors may be needed depending on activity levels [45].

Semiconductor grade single side mirror polished Ge wafers, supplied by University Wafers [46], with cleavage planes of $< 111 >$ (0.4 mm thick, $\rho \sim 30\ \Omega$ cm) and $< 100 >$ (1 mm thick, $\rho \geq 35\ \Omega$ cm) were taken for irradiation. These wafers were verified to be n-type by hot probe method [47]. Although the crystal orientation is not expected to have a strong effect on sensor properties, the Ge wafers with $< 100 >$ orientation are preferred for the ease of cleaving the samples for sensor fabrication. The Ge samples of varying sizes are irradiated at designated ports with thermal neutrons from Dhruva reactor at BARC, Mumbai. A detailed spectroscopic study of the NTD Ge samples [48] has been carried out in a special low background counting setup [49] to estimate the radioactive impurities. Chemical etching has been employed to remove the radioactive impurities implanted/diffused close to the surface and an assessment of trace radioactivity in bulk Ge has been carried out. An estimate of the cooldown period has been made based on these measurements. Dependence of radioactive impurities on neutron dose has been investigated. Effect of environment like wrapping material

has also been explored within permissible constraints. This chapter describes the experimental details and the radioactive impurity results from spectroscopy measurements.

2.1 Secondary Ion Mass Spectroscopy

The Time Of Flight Secondary Ion Mass Spectroscopy (TOF-SIMS) is employed to obtain the isotopic abundance with the ppm level sensitivity. The TOF-SIMS [50] was carried out at BARC laboratory [51, 52] using a 25 keV ^{69}Ga mono-isotopic Liquid Metal ion gun as the primary ion source with a final current density of about 0.03mA/cm^2 and a spot size of about 250 nm was achieved using suitable focusing lenses. Secondary ions produced through collision cascade mechanism were extracted with a wide acceptance angle which ensured that nearly every ion produced was extracted from the Ge sample surface. The Ge sample was pulsed at high potential (+2000 V_{dc}) which provided the acceleration energy for the secondary ions produced. A modified Wiley-Mclaren type reflectron was utilized to enhance the mass resolution. Grids at the entrance, middle and rear ensured that the reflection can be tuned in a single stage or double stage mode by modifying the electrostatic field gradients. The extracted ions with slightly

varying kinetic energies were reflected by the reflectron and were eventually time focussed onto a microchannel plate detector operated in the ion counting mode.

The ion signals after suitable amplification with a fast preamplifier were counted in a P7887 Fast ComTec (Germany) Multiscaler for generating the time spectrum, which was later converted into a Mass Spectrum. Figure 2.1 shows the mass spectrum of $< 111 >$ and $< 100 >$ oriented Ge samples. Selected mass peaks were fitted with a standard gaussian fit and the area under the curve was integrated to obtain the yield of the individual Ge isotopes. The measured isotopic abundances are listed in Table 2.1.

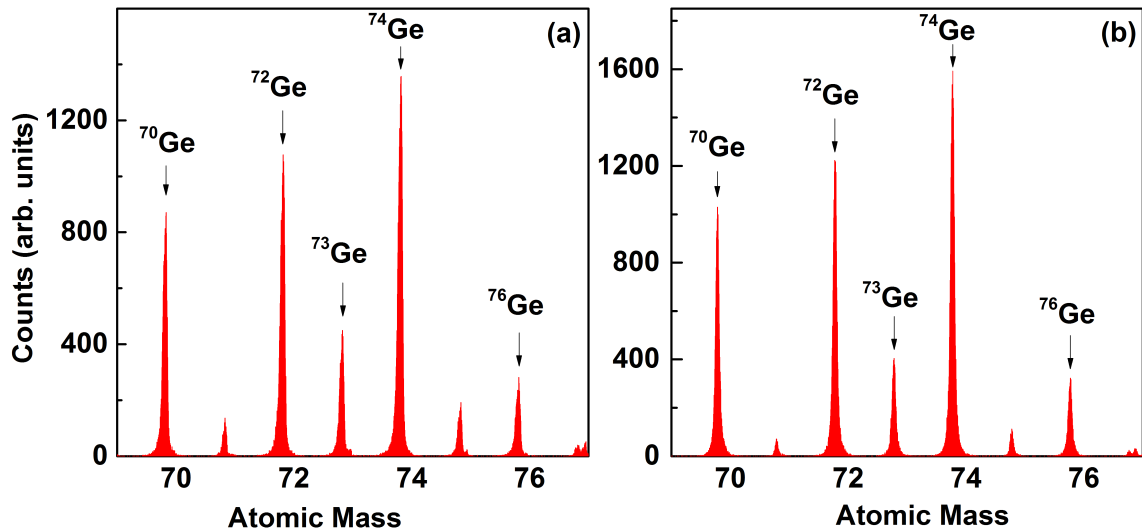

Figure 2.1: Mass spectrum from TOF-SIMS in A= 69 to 77 range for (a) $< 111 >$ Ge and (b) $< 100 >$ Ge sample.

Although overall composition is similar, small differences are present in the composition of $< 111 >$ and $< 100 >$ oriented wafers, which may depend on the crystal growth condition or the composition of the raw material. It should be mentioned that both $< 100 >$ and $< 111 >$ samples show a higher fraction of ^{73}Ge compared to the natural concentration. This may be a consequence of the starting material being enriched in ^{73}Ge, but further details are not available from the supplier. However, this is not relevant for the sensor development since ^{73}Ge does not contribute to the carrier concentration.

Table 2.1: Measured isotopic abundances of Ge in the wafers used, n-capture reaction and the stable end products are listed together with the decay mode and half-lives of products [53]. The natural concentration of Ge isotopes [54] is also included in column 2 for reference.

Isotope	Abundance(%)			(n,γ) reaction product and decay mode ($T_{1/2}$)
	Nat.	$<111>$	$<100>$	
^{70}Ge	20.6	21.5(0.2)	21.9(0.2)	$^{70}\mathrm{Ge} \rightarrow {}^{71}\mathrm{Ge} \xrightarrow{\mathrm{EC}(11.4\ \mathrm{days})} {}^{71}\mathrm{Ga}$
^{72}Ge	27.4	26.8(0.2)	27.0(0.2)	$^{72}\mathrm{Ge} \rightarrow {}^{73}\mathrm{Ge}$
^{73}Ge	7.8	10.8(0.1)	8.8(0.1)	$^{73}\mathrm{Ge} \rightarrow {}^{74}\mathrm{Ge}$
^{74}Ge	36.5	34.1(0.2)	35.1(0.2)	$^{74}\mathrm{Ge} \rightarrow {}^{75}\mathrm{Ge} \xrightarrow{\beta^-(82.8\ \mathrm{min})} {}^{75}\mathrm{As}$
^{76}Ge	7.7	6.8(0.1)	7.2(0.1)	$^{76}\mathrm{Ge} \rightarrow {}^{77}\mathrm{Ge} \xrightarrow{\beta^-(11.3\ \mathrm{hr})} {}^{77}\mathrm{As} \xrightarrow{\beta^-(38.8\ \mathrm{hr})} {}^{77}\mathrm{Se}$

The production rate of dopants are estimated from the measured isotopic abundances (Table 2.1) using n-capture cross sections from Ref. [55] and are tabulated Table 2.2 together with the expected net carrier concentration.

Table 2.2: Estimated production rate of dopants (atoms/cm^3) per neutron, obtained by multiplying measured isotopic abundance of Ge with n-capture cross section (taken from Ref. [55]).

Sample	^{71}Ga	^{75}As	^{77}Se	*Net carrier concentration
<111>	3.23×10^{-2}	7.78×10^{-3}	4.76×10^{-4}	2.35×10^{-2}
<100>	3.32×10^{-2}	7.89×10^{-3}	5.08×10^{-4}	2.43×10^{-2}

*Net carrier concentration (p-type) = ^{71}Ga - (^{75}As + 2 $\times$ ^{77}Se)

2.2 Neutron Irradiation

Prior to irradiation, samples were cleaned in an ultrasonic bath with electronic grade isopropyl alcohol for about 15 min and blow dried with dry N_2. Samples were loaded in a specially designed capsule as per the mandatory procedure for irradiation in the Dhruva reactor. Different mounting arrangements permissible within operational constraints of the irradiation process in the reactor were tried out to assess the effect of wrapping material and irradiation environment. These consisted of a single sample wrapped in Aluminium foil (Pari, Switzerland, thickness 4.58 mg/cm^2), three stacked samples wrapped in a common Aluminium foil, three stacked samples inside a commercial quartz tube and three sample stacked in a vacuum sealed quartz tube. The quartz tube was also wrapped with Aluminium foil. Figure 2.2 shows the samples prepared for irradiation. Both Aluminium and

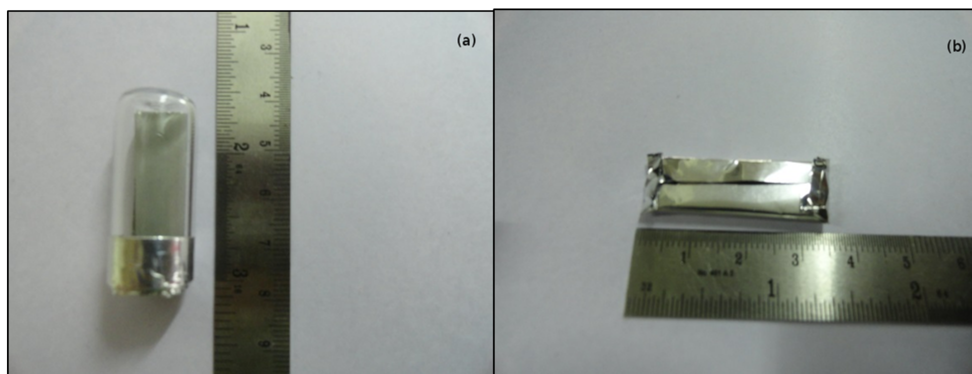

Figure 2.2: Ge samples packed in (a)quartz tube and (b) in Al wrapper for neutron irradiation.

quartz are permissible materials at the Dhruva reactor as the flux attenuation is minimal and there is no resultant long term activity in the wrapping material. In most cases the maximum permissible sample size of 30 mm $\times$10 mm was used. In case of quartz sealed sample, a smaller size of 10 mm $\times$10 mm was used in order to avoid melting of Ge wafers while sealing the quartz tube. The irradiation details like sample sizes and wrapping materials are given in Table 2.3. Samples A, B, C are of $< 111 >$ type while all others (D to I) are of $< 100 >$ type. The samples were finally placed inside a cold sealed Aluminium tube capsule (2 cm dia, 4 cm height) for irradiation. In the Dhruva reactor, irradiations are done at fixed positions inside the reactor core and the neutron flux is assumed to be uniform. The neutron fluence is estimated from the reactor power and is given in Table 2.4. In the Dhruva reactor, the relative yields of epithermal and fast neutrons (E $>$ 0.8 MeV) with respect to thermal neutron yields, are $\sim$ 20% and $\sim$ 1%, respectively. For

Table 2.3: Details of the irradiated Ge samples

Ge samples (Plane, Resistivity)	Tag	Dimension (size in mm^2)	nos.	Wrapping details
Set 1 ($< 111 >$, $> 30\Omega cm$)	B	(10 x 10 x 0.4)	-	Al foil
	C	(10 x 10 x 0.4)	-	Al foil
Set 2 ($< 100 >$, $> 35\Omega cm$)	D(T1, M1, B1)	(30 x 10 x 1)	3	quartz tube
	D(T2, M2, B2)	(30 x 10 x 1)	3	Al foil
	E(T3, M3, B3)	(30 x 10 x 1)	3	quartz tube
	E(T4, M4, B4)	(30 x 10 x 1)	3	Al foil
	F (T5, M5, B5)	(30 x 10 x 1)	3	quartz tube
	G(T6, M6, B6)	(30 x 10 x 1)	3	Al foil
	H(1, 2, 3, 4, 5)	(10 x 10 x 1)	3	sealed quartz tube
	I(1, 2, 3)	(10 x 10 x 1)	3	Al foil

a more accurate dose measurement, it would be desirable to use a neutron dose monitor (e.g. Fe, Zr, Ni).

Table 2.4: Neutron fluence for different Ge samples

Sample Tag	Mean date of irradiation (t_0)	t_{irr} (days)	Neutron fluence (n/cm^2) Thermal $\times 10^{18}$	Epithermal $\times 10^{17}$	Fast $\times 10^{16}$
A	03/07/2011	4.0	2.76	8.64	2.76
B	11/08/2012	4.1	14.0	25.6	17.2
C	11/08/2012	4.1	9.13	17.2	11.2
D	13/09/2013	5.7	4.57	8.02	5.32
E	16/11/2013	4.1	2.11	3.52	2.46
F	21/11/2013	6.8	3.52	5.87	4.11
G	15/05/2014	6.9	3.57	5.95	4.16
H	10/05/2014	3.5	1.8	3.01	2.1
I	10/05/2014	3.5	1.8	3.01	2.1

After a cooldown period of $\sim$ 45 days, individual samples were removed from the irradiation capsule and carefully transferred to separate plastic pouches for spectroscopic measurements. In case of stacked samples, the label M (middle) refers to middle sandwiched sample while T (top) and B (bottom) refer to the outer samples. Some of the larger samples were cut into $\sim$ 1 cm $\times$ 1 cm size pieces after irradiation, which were labeled as L (left), C (center) and R (right). Measured activity of the sample with the highest neutron dose was $\sim$ 3 μSv/hr. It should be mentioned that irradiated samples often showed a lack of the lustre and significant improvement was observed after cleaning the NTD Ge samples with HF (40 %).

2.3 Radioactive Impurity Measurements

A specially designed Tifr Low background Experimental Setup (TiLES) at TIFR, consisting of $\sim$ 70 % HPGe detector surrounded by low activity Cu + Pb shield [49] was used for detection of characteristic γ-rays of radioactive impurities in the irradiated targets. Data were recorded with a commercial FPGA based 100 MS/s digitizer (CAEN-N6724). Depending on the activity of the sample, counting was done initially at 10 cm from the detector face and later in a close geometry with the sample directly mounted on the detector face. Concentrations of radioactive impurities were obtained from the intensity of the observed γ-rays after correcting

for efficiency, branching ratio and decay during the time elapsed since irradiation. The detection efficiency of a photon of given energy is obtained from MC simulations using the detector model as described in Ref. [49]. In close geometry, efficiency corrections due to coincident summing were taken into account. Spectra were recorded for 30 minutes to 24 hours of counting time. Spectra for the environmental radioactivity and virgin samples were recorded for reference and are shown in Figure 2.3. It should be mentioned that no additional trace impurities were visible in the virgin sample at measured sensitivity. Spectra of the irradiated Aluminium wrapper and the quartz tube were also studied separately. Figure 2.4 shows γ-ray spectra of the irradiated sample E-T3L (10×10 mm^2) after 125 days of cooldown time. The environmental radioactivity spectrum is also shown for comparison. Most of the n-capture products of Ge are either stable or have relatively short half-life compared to the initial cooldown period (45 days). The ^{71}Ge has a half-life of 11.4 days and decays mainly by electron capture to the ground state of ^{71}Ga. However, a small fraction that undergoes Radioactive Electron Capture (REC) [56] shows up as a continuous gamma spectrum of ^{71}Ge, which is observed with an endpoint energy of 225 keV. The gamma rays of ^{110m}Ag and ^{65}Zn are also visible in the lower panel.

Figure 2.5 shows a comparison of γ-ray spectra for the sample wrapped with Al foil (D-T2, red solid line) and the sample in quartz tube (D-T1, black

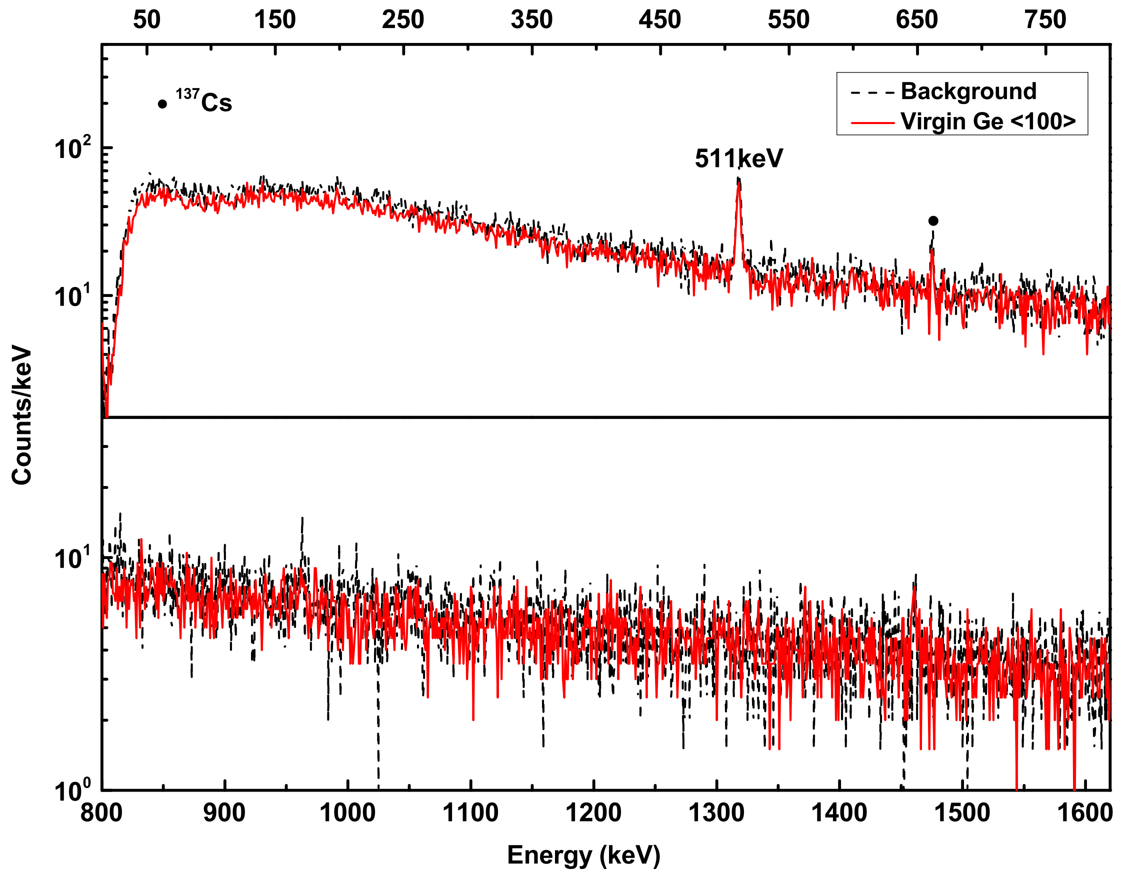

Figure 2.3: Gamma ray spectra of the $< 100 >$ virgin Ge sample (red solid line) for E_γ = 0 to 800 keV (top panel) and E_γ = 800 to 1600 keV (bottom panel) together with that of the ambient background (black dotted line). Both the spectra are normalized to 12 hours counting time.

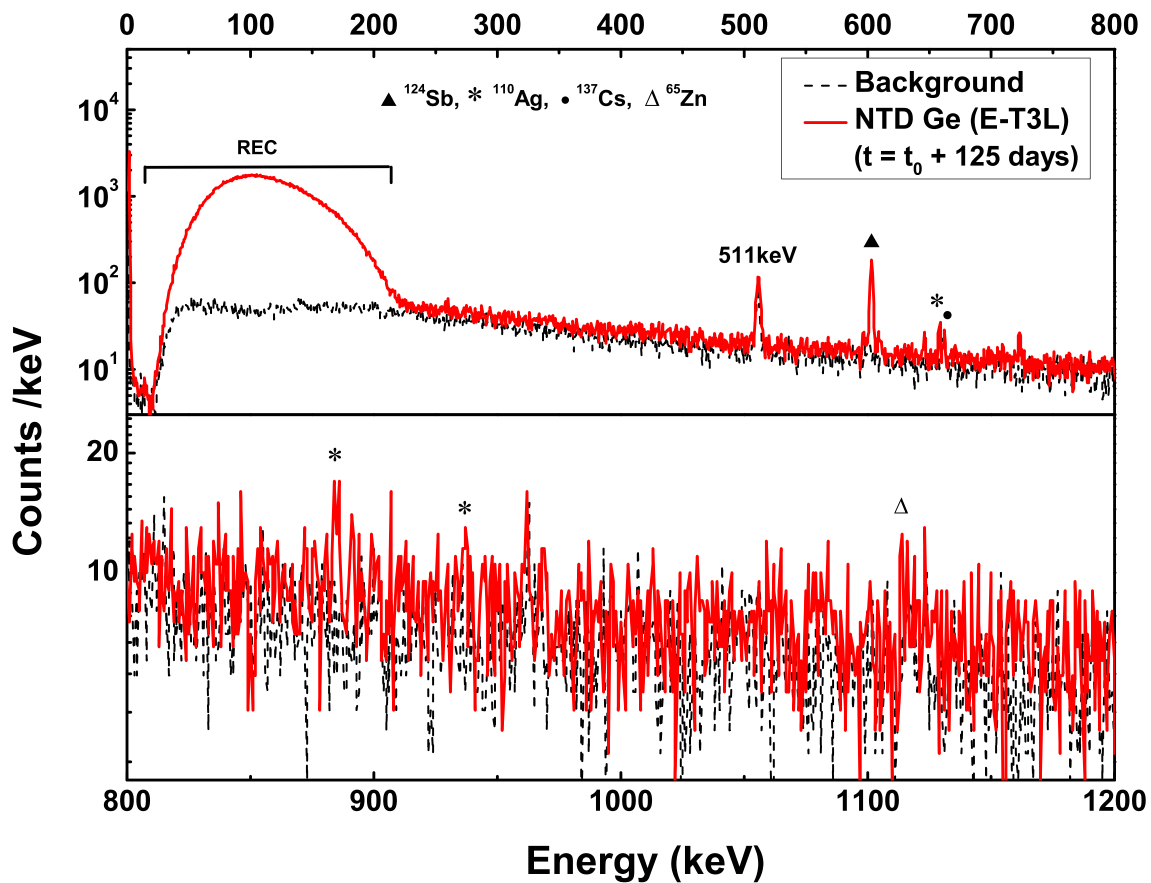

Figure 2.4: Gamma ray spectra of sample E-T3L (red solid line), for 12 hours of counting time.

dotted line) after a cool down period of 36 days. It can be clearly seen that the Ge sample wrapped with Al foil shows higher ^{110m}Ag contamination compared to the one in the quartz tube.

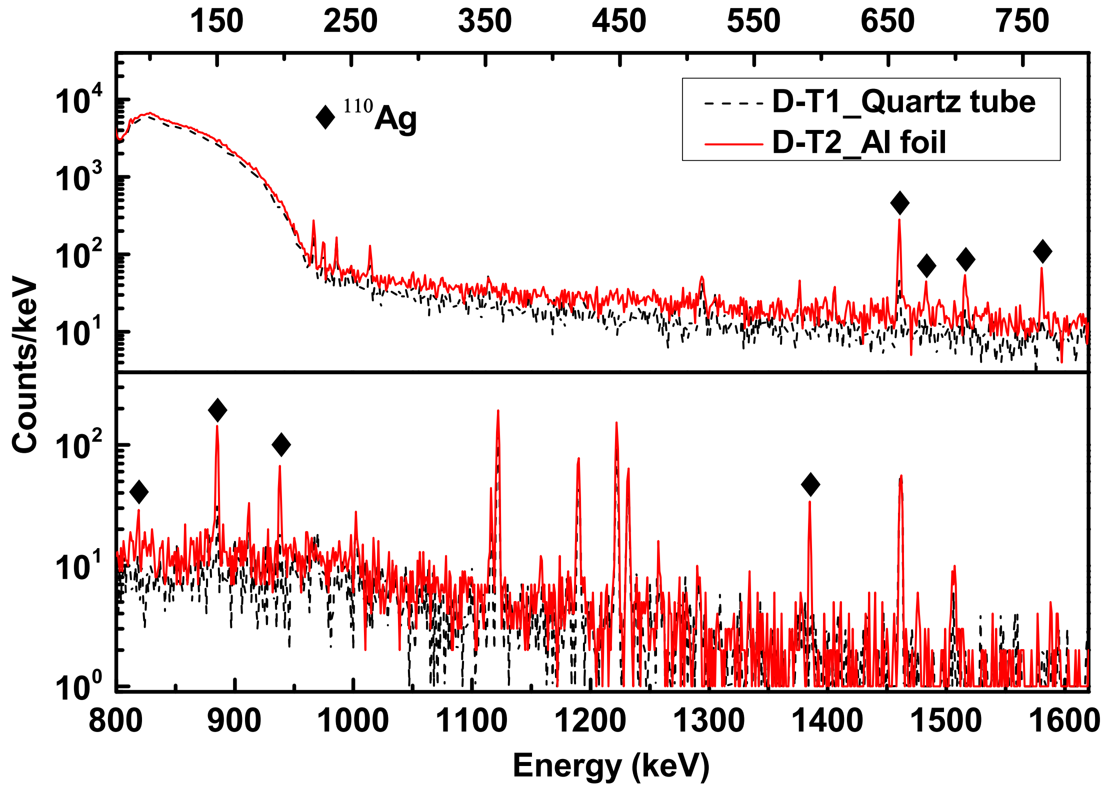

Figure 2.5: Gamma ray spectra of sample D-T1 in quartz tube (black dotted line) and Al foil wrapped sample D-T2 (red solid line) at t = t_0 + 36 days, for 30 minutes of counting time.

Table 2.5 lists the observed radionuclides in various samples together with half-lives, prominent γ-rays and relative intensities. For unambiguous identification, half-lives of the observed γ-rays were measured and have been found to be consistent within 10 %. In addition, wherever applicable,

Table 2.5: A list of radionuclides and characteristic γ-rays observed in NTD Ge samples before etching.

Radionuclide	Half-life	E_γ (keV)	Relative Intensity (%)
^{46}Sc	83.79 d	889.3	99.98
		1120.5	99.99
^{51}Cr	27.7 d	320.1	9.91
^{59}Fe	44.5 d	1099.3	56.5
		1291.6	43.2
^{60}Co	5.27 y	1173.2	99.85
		1332.5	99.98
^{65}Zn	243.66 d	1115.5	50.04
^{110m}Ag	249.76 d	657.8	95.61
		884.7	75.0
		937.5	35.0
^{124}Sb	60.2 d	602.7	97.8
		1691.0	47.57
		722.8	10.76
^{182}Ta	114.74 d	1121.3	35.24
		1221.4	27.23
		1231.0	11.62

relative intensities of multiple γ-rays of the given nuclide were also verified. As is evident from the table most of these nuclides are fairly long lived and hence a cause of major concern for low background studies.

To investigate the depth dependence of radioactive impurities, the NTD Ge samples were chemically etched in a controlled manner using H_2O_2 in an ultrasonic bath at 80°C [57] up to a depth of $\sim$ 50 μm. Samples were cleaned in HF before and after H_2O_2 etching to remove oxide layers. Typical etching rate observed was 0.3 μm/min and etched depth was estimated by accurate mass measurement of the sample assuming uniform etching from all sides.

It should also be mentioned that for n-induced reaction products from wrapping material to get implanted in Ge sample, reactions must take place close to the surface of the wrapping material. Hence, the surface trace impurities in wrapping materials were separately studied ($\sim$ few μm depth) using Energy Dispersive X-ray Analysis (EDAX) [58].

2.4 Analysis of Radioactive Impurity Data

There are four possible sources of radioactive impurities: 1) neutron induced reaction products of impurities in bulk Germanium, 2) neutron induced reaction products of residual impurities in the Ge surface (resulting from contamination during lapping/polishing/cutting), 3) neutron induced

reaction products from wrapping material which can get recoil implanted in Ge and 4) deposition and thermal diffusion of radioactive contaminants from the surrounding environment in the sample capsule resulting from long exposures at high temperatures during irradiation ($\sim 80^{\circ}$C).

Contamination deposited on the irradiated Ge sample was removed by rinsing the sample with HF. A comparison of γ-ray spectra for the G-T6 sample before and after HF cleaning is shown in Figure 2.6. It is evident that the HF cleaning has considerably reduced the radioactive impurities like ^{60}Co, ^{65}Zn and ^{182}Ta, indicating that these are surface deposits.

Figure 2.7 shows γ-ray spectra of the NTD Ge samples before (red solid line) and after (black dotted line) etching with H_2O_2 for (a) sample D-B1 and (b) sample I-L. The sample D-B1 was exposed to the highest neutron fluence ($\Phi_{th} = 4.6 \times 10^{18}/\mathrm{cm}^2$) in the $< 100 >$ set and clearly shows significantly higher activity as compared to the E samples (shown in Figure 2.4). The REC continuum at low energy is not visible due to larger cooldown time. In the spectra of the etched samples, it is clearly seen that most of the prominent γ-rays from the surface impurities are below measurable limits, while γ-rays from the bulk impurities (^{124}Sb) are visible above the background. The 511 keV which is a prominent peak in all the spectra is the annihilation peak of positron. The main sources are the β^{+}-decay from the isotopes such as ^{208}Tl and ^{40}K present in the environment

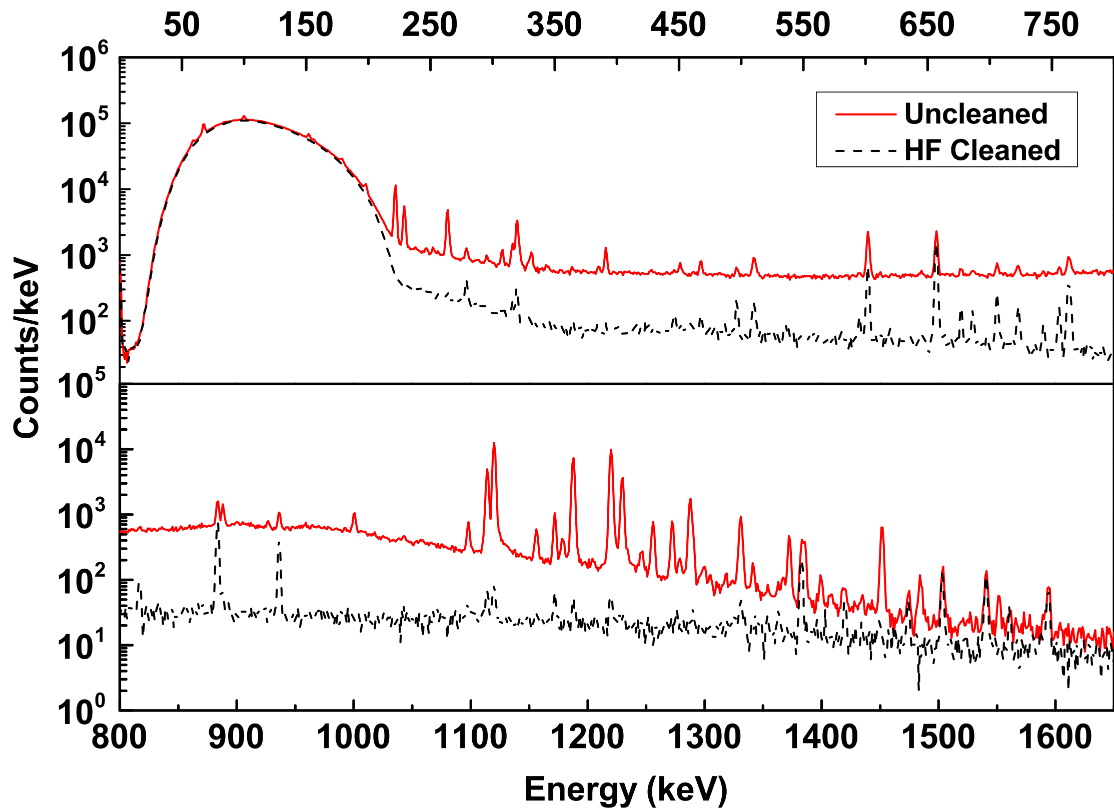

Figure 2.6: Gamma ray spectra of sample G-T6 before (red solid line) and after HF cleaning (black dashed line) at t = t_0 + 63 days, for 2 hours of counting time.

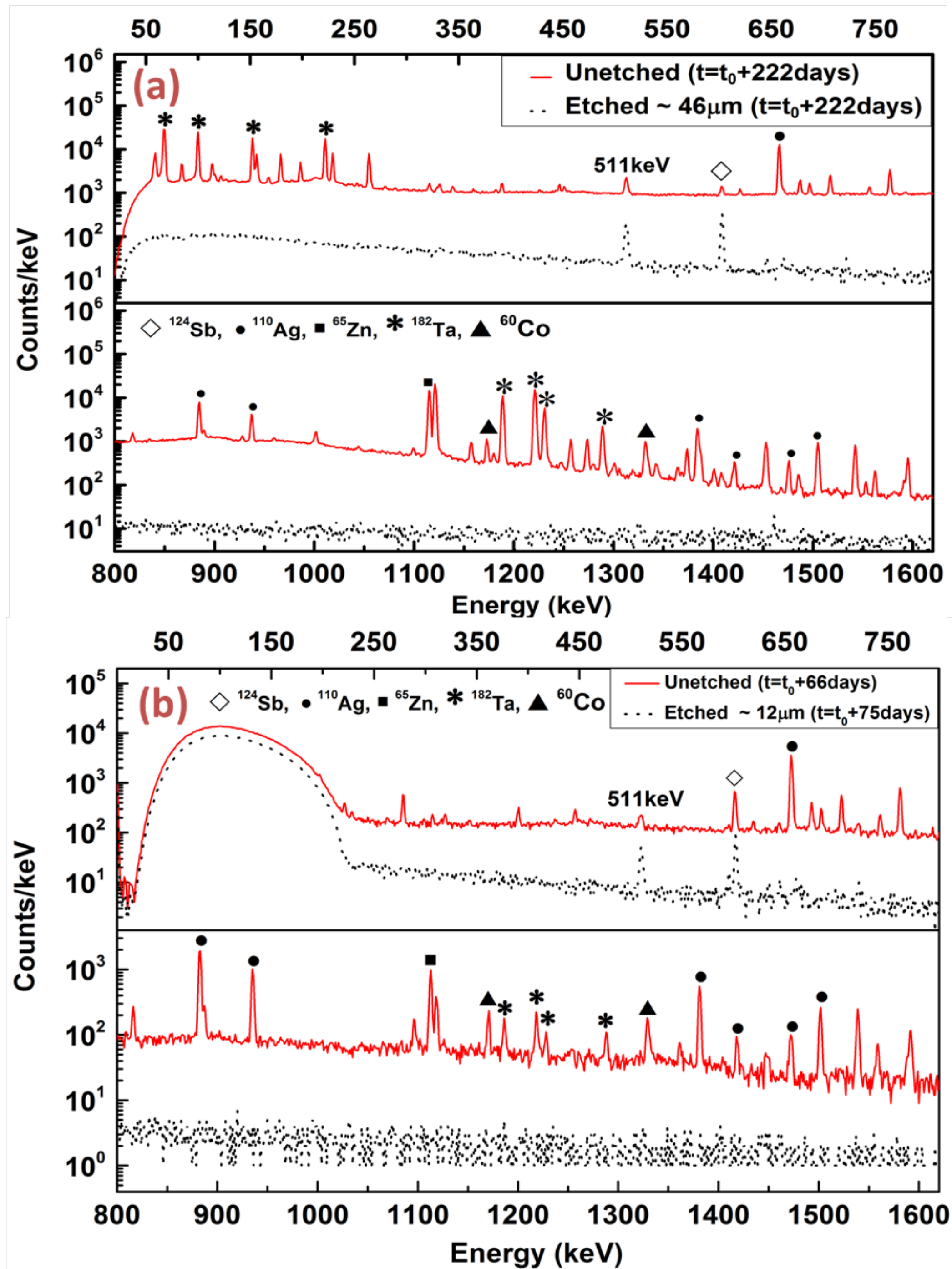

Figure 2.7: Gamma ray spectra before (red solid line) and after (black dotted line) etching for (a) sample D-B1 for 12 hours of counting time and (b) sample I-L for 3 hours of counting time.

For understanding the origin of radioactive impurities, the observed ^{110m}Ag activity normalized with respect to the surface value is shown in the Figure 2.8 as a function of etching depth for the samples B $< 111 >$ and D-M2L $< 100 >$. In both the samples, there is a sharp decrease in the activity near the surface, but a significant reduction is seen only after about 5 μm of the etching depth. In case of sample B, ^{110m}Ag activity was found to remain constant after 10 μm depth whereas for the sample D-M2L there was no measurable Ag activity after 15 μm etching.

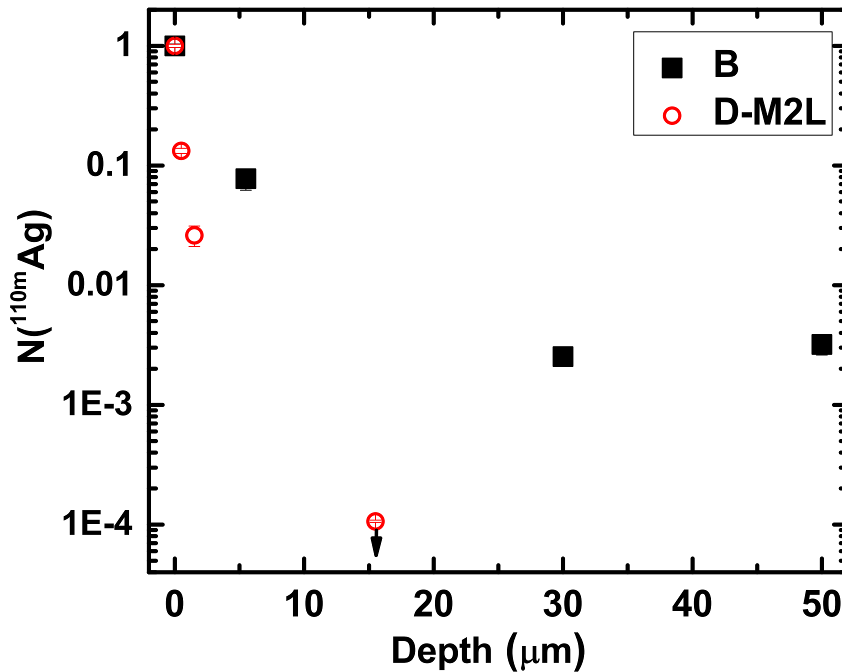

Figure 2.8: The ^{110m}Ag activity normalized with respect to the surface value as a function of etching depth for the samples B $< 111 >$ and D-M2L $< 100 >$. Errors are smaller than symbol size and arrow indicates the activity below the detection limit.

To eliminate the possibility of radioactive impurities getting implanted from the surrounding material, spectroscopic studies on Ge samples sealed in quartz tube were carried out. Figure 2.9 shows the γ-ray spectra for the H4 sample before surface cleaning, after HF cleaning and after 10 μm etching with H_2O_2. No significant improvement was observed in the sample sealed in a quartz tube.

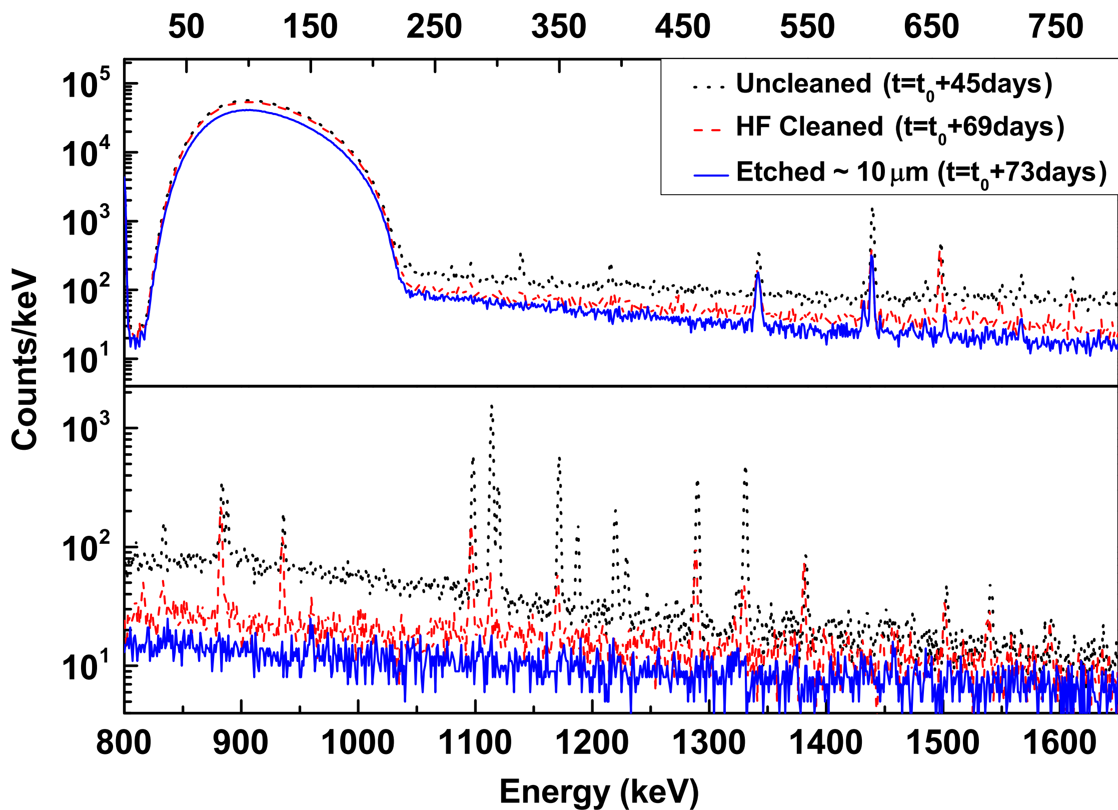

Figure 2.9: Gamma ray spectra of the sample H4 before etching (black dotted line), after HF cleaning (red dashed line) and after 10 μm etching with H_2O_2 (blue solid line), for 90 minutes of counting time.

Table 2.6 gives a summary of the observed radioactive impurities at various etching depths (d) in different samples. For most of the samples, the activities of ^{65}Zn and ^{60}Co reduced significantly after etching of few μm surface layer. In some cases, low level activity became visible after surface level etching (e.g. ^{65}Zn in E-T3L) due to the improved background.

Since implanted impurities will be restricted to sub-micron layers near the surface, the observation of activities up to 10 μm layer is surprising and not easy to understand. This could result from thermal diffusion of impurities which will depend on both temperature and time (Ref. [59]). Given the time scale of neutron irradiation ($\sim$ 4 to 5 days) at 80°C there might be a possibility of heavy nuclei like Ag thermally diffusing at the micrometer scale. The surface contamination during the wafer processing stage is also a possibility. It should be mentioned that even in case of D samples, which had highest neutron fluence amongst $< 100 >$ set ($\Phi_{\text{th}} \sim 4.6 \times 10^{18}/\text{cm}^2$), some traces of ^{110m}Ag and ^{182}Ta could be seen till 40 μm depth. No measurable activity was found in the NTD A sample, which had a nearly 3 years of cooldown time. However, since a very small size sample ($\sim$ 15 mg) was used for spectroscopic studies, no limits on radiopurity of the sample were extracted. Samples from $< 111 >$ (B, C) and from $< 100 >$ (D-I) showed different bulk impurities. The only measurable radioactivity present in $< 100 >$ Ge after $\sim$ 50 μm etching was ^{124}Sb. While the ^{124}Sb

Table 2.6: Observed radioactive impurities as a function of the etched depth (d) in different samples. When data is not available corresponding to a given etching depth, the cells are left blank.

Sample	observed radio-nuclides		
	d = 0 μm	d = 5–20 μm	d = 40–60μm
B	^{60}Co, ^{65}Zn, ^{110m}Ag, ^{182}Ta	-	^{110m}Ag
C	^{60}Co, ^{65}Zn, ^{110m}Ag, ^{182}Ta	-	^{110m}Ag
D-T1	^{60}Co, ^{65}Zn, ^{110m}Ag, ^{124}Sb, ^{182}Ta	^{60}Co, ^{110m}Ag, ^{124}Sb	^{124}Sb
D-M2L	^{60}Co, ^{65}Zn, ^{110m}Ag, ^{124}Sb, ^{182}Ta	^{124}Sb	-
D-B1	^{60}Co, ^{65}Zn, ^{110m}Ag, ^{124}Sb, ^{182}Ta	^{124}Sb, ^{110m}Ag	^{124}Sb
E-T3L	^{124}Sb, ^{110m}Ag	^{124}Sb, ^{65}Zn	^{124}Sb
F-B5	^{124}Sb, ^{110m}Ag, ^{65}Zn	^{124}Sb	^{124}Sb
G-T6	^{46}Sc, ^{51}Cr, ^{60}Co, ^{65}Zn, ^{110}Ag, ^{124}Sb, ^{182}Ta	^{124}Sb	-
H4	^{46}Sc, ^{51}Cr, ^{60}Co, ^{65}Zn, ^{110}Ag, ^{124}Sb, ^{182}Ta	^{124}Sb	^{124}Sb
I-L	^{46}Sc, ^{51}Cr, ^{60}Co, ^{65}Zn, ^{110}Ag, ^{124}Sb, ^{182}Ta	^{124}Sb	-

activity was not seen in $< 111 >$ Ge samples, they showed activities of ^{65}Zn (222 ± 87 mBq/g) and ^{110m}Ag (225 ± 67 mBq/g) even after 50 μm etching and ~ 1.6 years of cooldown period.

Table 2.7 lists the measured activities for various NTD Ge samples, 150 days after the irradiation. The etched samples from $< 100 >$ set did not

Table 2.7: Measured radioactivity and estimated cooldown period (T_{cool}) for reduction of the radio-activity below < 1 mBq/g for various NTD Ge samples. Detection limits are indicated, wherever the activity could not be measured above the background.

Sample	Activity (mBq/g) (t_0 + 150 days)		T_{cool} (yr)
	^{110m}Ag	^{124}Sb	
B	3018(465)	< 26.6	9
C	743(222)	< 18.6	7
D-B1	< 2.0	420(9)	1.9
E-T3	< 2.5*	201(20)	1.7
F-B5	< 2.9	344(12)	1.8
G-T6	-	425(7)	1.9
H4	-	175(9)	1.7
I-L	-	185(17)	1.7

* Estimated from sample E-T3L

show any measurable ^{110m}Ag activity and only detection limits are mentioned. In Ref. [45], which reports the sensor development for CUORE experiment, it is mentioned that the residual activity of ≥ 1mBq/g after 3 years is of significant concern. Hence in the present work, we have estimated the required cooldown time to achieve a similar level of activity,

which is listed in the last column. It is evident that for $< 100 >$ samples (D-I), with the expected dose $\Phi_{\rm th} \sim 1-5 \times 10^{18}/{\rm cm}^2$, approximately 2 years of cooldown period after irradiation is essential. The higher radioactivity levels of ^{110m}Ag in samples B and C indicate that material from these samples will be unsuitable for sensors in the low counting experiment. Further, since the neutron fluence of samples B and C are higher than 5×10^{18} n/cm^2 (as given in Table 2.4), these samples will be near metallic and are unsuitable for sensor fabrication. It should be mentioned that the commercial NTD Ge sensor (AdSem, Inc [60]) showed much higher levels of ^{65}Zn and ^{110m}Ag, possibly due to other materials used in contact fabrication.

As mentioned earlier, Alessandrello *et al.* [45] have also measured the residual radioactivity in NTD Ge thermistors for a similar neutron fluence, namely, $\Phi_{\rm th} \sim 3.36 \times 10^{18}/{\rm cm}^2$. They have reported several isotopes like ^{75}Se, ^{74}As and ^{68}Ge resulting from fast neutron induced reactions during irradiation. Elliott *et al.* [61] have also reported the formation of isotopes like ^{65}Zn, ^{54}Mn and ^{60}Co in high energy neutron induced reactions. In the present case though ^{65}Zn activity was seen at surface of the samples, the γ-rays corresponding to fast neutron induced reaction products (namely, ^{75}Se, ^{74}As, ^{68}Ge, ^{54}Mn, ^{60}Co and ^{65}Zn) are not visible in the irradiated-etched samples. The detection limits on activities of ^{75}Se, ^{74}As, ^{68}Ge for the sample F-B5 at t$\sim t_0$+150 days are given in Table 2.8 together with the values

reported in Ref. [45], measured immediately after the irradiation. While the limit on ^{68}Ge activity is lower in the present case, the ^{74}As activity is similar to that in Ref. [45]. The detection limit for the ^{75}Se activity in the present case is significantly worse than the measured value of Ref. [45]. It should be noted that present measurements are carried out after a cooldown time of $\sim$ 150 days, where the short lived activities like ^{74}As would have significantly decayed. Also, the yield of (n,α) or (n,3n), (n,p) reactions responsible for ^{75}Se and ^{68}Ge production will depend on high energy neutron flux, which can be different in two cases.

Table 2.8: Estimated limits on fast neutron induced reaction products in Ge for sample F-B5 after a cooldown period of 150 days. Data from Ref. [45] immediately after irradiation is also shown for comparison.

Radionuclide	Possible reactions	$T_{1/2}$ days	Present detection limit mBq/g	Data from Ref. [45] mBq/g
^{68}Ge	^{70}Ge(n,3n), ^{72}Ge(n,5n)	270	$<$51	150(10)
^{75}Se	^{72}Ge(α,n), ^{73}Ge(α,2n), ^{74}Ge(α,3n)	119.78	$<$15.2	3.3(0.8)
^{74}As	^{74}Ge(p,n), ^{73}Ge(n,γ)	17.72	$<$2.8	4400(750)
^{60}Co	^{59}Co(n,γ)	1925.28	$<$1.9	-

Effects of impurities were also investigated by carrying out HF cleaning and H_2O_2 etching prior to neutron irradiation. Preliminary results on samples etched prior to irradiation show significant improvement, indicating the possibility of surface contamination due to mechanical etching/polishing process. It should be mentioned that simple HF cleaning before irradiation did not show any reduction in radioactive impurities.

The EDAX analysis of Aluminium wrapper and the quartz tube had shown a purity level of $\sim$ 99%. The irradiated Aluminium wrapper showed very high levels of ^{110m}Ag, ^{65}Zn and ^{182}Ta, while the quartz tube showed several additional γ-rays of ^{54}Mn, ^{58}Co and ^{134}Cs. Any reaction products originating from (n, γ), (n, α), (n, p) reactions on ^{27}Al result in stable/short-lived products such as ^{28}Al ($T_{1/2}$ = 2.2 m), ^{24}Na ($T_{1/2}$ = 15 h) and ^{27}Mg ($T_{1/2}$ = 9.5 m), respectively. Hence these short-lived products could not be observed after $\sim$ 45 days. For a neutron fluence of $\Phi_{th} \sim 4.6 \times 10^{18}/cm^2$, the measured ^{110m}Ag activity in the Aluminium wrapper and the quartz was $\sim$ 2.2 kBq/g (corresponding to $\sim$ 0.2 ppm of ^{109}Ag in ^{nat}Al) and $\sim$ 0.07 kBq/g (corresponding to $\sim$ 0.02 ppm of ^{109}Ag in SiO_2), respectively, after a cool down period of $\sim$ 150 days. The surface activity of ^{110m}Ag (Figure 2.5) in the corresponding Ge samples, namely, D-T2 (wrapped in the Aluminum)

and D-T1 (in the quartz tube) was 56(2) Bq/g and 7.2(0.4) Bq/g, respectively. It is evident that the Ge samples wrapped in Aluminium showed higher surface activity as compared to those in the quartz tube.

2.5 Estimation of Φ_{th} from ^{124}Sb

The observed residual activity of ^{124}Sb results predominantly from the ^{123}Sb(n,γ) reaction with thermal neutrons. The contribution from the fast neutrons can be neglected since the flux for $E_n > 1$ MeV is smaller by a factor $\sim$ 100 and the cross-section for n-capture is smaller by a factor of $\sim$ 50. The concentration of the reaction product is related to that of the parent isotope ($N_{impurity}$) by the following relation:

$$N_{\gamma}^{product} = \frac{N_{impurity} \times \sigma_c \times \phi_{\mathrm{th}} \times (1 - e^{-\lambda t_{irr}})}{\lambda} \tag{2.1}$$

where σ_c is the thermal neutron capture cross-section (to the ground state and/or excited state as the case may be) [55], λ is the decay constant, t_{irr} is the duration of the irradiation and ϕ_{th} is the thermal neutron flux expressed in units of neutrons.cm^{-2}.s^{-1}. The ϕ_{th} is assumed to be uniform during the irradiation period, i.e. $\phi_{\mathrm{th}} = \Phi_{\mathrm{th}}/\mathrm{t}_{\mathrm{irr}}$.

The $N_\gamma^{product}$ is computed from the measured intensity of γ-ray (N_γ) during the counting time interval of t_1 to t_2 (measured with respect to end of the irradiation) and is given by

$$N_\gamma^{product} = \frac{N_\gamma}{\varepsilon_\gamma \times I_\gamma \times (e^{-\lambda t_1} - e^{-\lambda t_2})} \tag{2.2}$$

where ε_γ and I_γ are the photopeak detection efficiency and branching ratio of the γ-ray, respectively.

Table 2.9 lists the estimated bulk impurity concentration of ^{123}Sb from the observed activity of ^{124}Sb using equations 1 and 2. The isotope ^{121}Sb, which is more abundant, produces short-lived activity ($\sim$ 2.7 days) and could not be observed in the present studies. However, considering the presence of ^{123}Sb in Ge as indicative of ^{nat}Sb and assuming the natural abundances for ^{121}Sb and ^{123}Sb (57% and 43%, respectively [54]), the bulk impurity of ^{nat}Sb in $< 100 >$ Ge is estimated to be 277(14) ppt.

Table 2.9: Estimated traces of ^{123}Sb impurities from the residual radioactivity of ^{124}Sb in etched $< 100 >$ NTD Ge samples. The etched depth for each sample is indicated in the bracket. Systematic errors in detector efficiency (about 5 %) [49] are not included and only statistical errors are shown.

Parent isotope	$E_\gamma^{product}$ (keV)	Concentration (ppt) D-B1 (46 μm)	E-T3L (42 μm)	F-B5 (52 μm)	G-T6 (5 μm)	H4 (40 μm)	I-L (12 μm)
^{123}Sb	602.7	115(2)	119(12)	123(4)	149(3)	122(6)	130(12)

Figure 2.10 shows a plot of relative neutron fluence (R) of sample D, F, G and H with respect to the E sample extracted from ^{124}Sb activity (open square) and from the irradiation data (filled circle). The good agreement

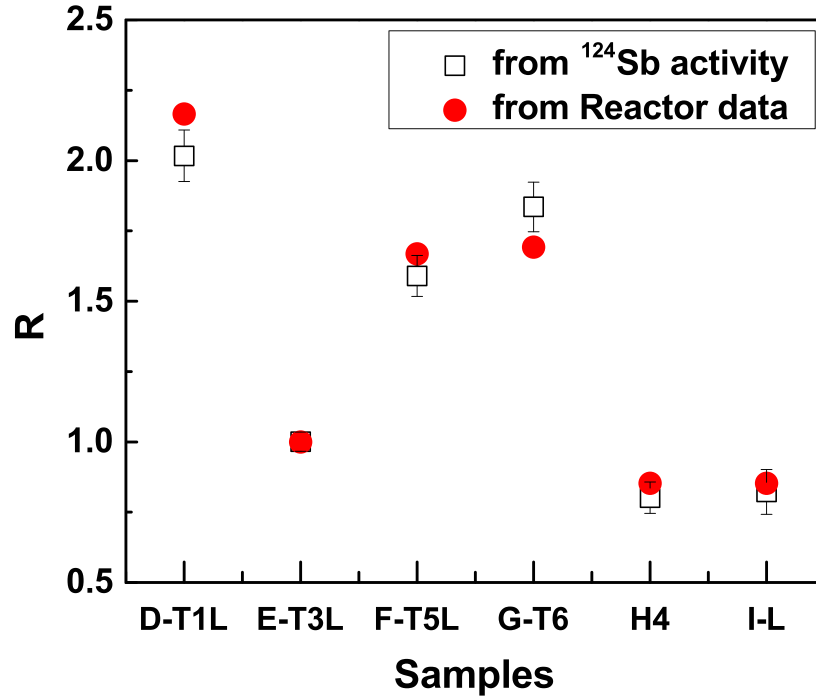

Figure 2.10: Relative neutron fluence (R) of samples D, F, G, H and I with respect to the sample E from the residual ^{124}Sb activity (open square) and from the irradiation data (filled circle).

between these two indicate that the observed bulk impurity concentration of ^{123}Sb is similar in different samples of $< 100 >$. It may be noted that the observed bulk impurity level of ^{123}Sb $\sim$ 100 ppt is much below the sensitivity of SIMS (ppm) and hence could not be measured in the SIMS. Further, Alessandrello et al. [45] have reported much smaller bulk impurity concentration of ^{123}Sb in Ge, namely, < 1 ppt. The ^{123}Sb impurity needs

to be minimized as it leads to high energy gamma ray background ($E_\gamma >$ 2 MeV) and moreover, it determines the required cool down period of the sensor in the present case. Therefore, it would be desirable to use detector grade Ge as a starting material instead of the device grade Ge wafer.

2.6 Summary

Radioactive impurity studies in NTD Ge samples have been performed. The semiconductor grade Ge wafers of cleavage planes $< 111 >$ (0.4 mm thick, $\rho \sim 30\ \Omega$ cm) and $< 100 >$ (1 mm thick, $\rho \geq 35\ \Omega$ cm) were taken for these studies. The isotopic abundance of the Ge samples was obtained with TOF-SIMS technique at BARC. Neutron irradiation has been carried out with thermal neutron fluence in the range 1.8×10^{18} to $1.4 \times 10^{19}/\mathrm{cm}^2$ at Dhruva reactor, BARC. Irradiated Ge samples were studied for impurities in the low background counting setup (TiLES) and all peaks in the γ-spectra were identified. Chemical etching of the surface removed most of the long lived impurities, indicating that these impurities can arise either from residual surface contamination of the sample or due to diffusion during irradiation from the sample capsule environment. Generally the samples loaded in the quartz tube were found to have lower radioactivity than those wrapped in Aluminium. Spectroscopic studies of the Ge sample sealed in quartz tube did not show significant improvement in the level of radioactive impurities.

Preliminary results of Ge samples etched prior to irradiation have shown promising results. The chemical etching after irradiation does not affect the performance of the sensor but is desirable even from thermometry consideration since radioactive impurities can act as a standing heat load at mK temperature. For the desired neutron fluence of $1-5 \times 10^{18}$/cm^2, removal of 50 μm surface layer is found to be adequate. The observed radioactive impurities ~ 1 Bq/g in the bulk Ge, estimated after chemical etching of the samples, implies that a cooldown period of ~ 2 years would be necessary before sensors made from these samples can be used in rare decay studies requiring ultra low background (≤ 1 mBq/g). In order to reduce bulk radioactive impurities, detector grade Ge wafers will be desirable.

Chapter 3

Defect studies in NTD Ge

During irradiation, Ge samples are exposed to neutrons having a broad range of energies (< 0.625 eV to 10 MeV) since reactor neutrons are not mono-energetic. High energy neutrons, in particular, can cause damage to the lattice structure of the crystal. Even for thermal neutrons, the average recoil energy ($\sim$ 182 eV) of Ge(n,γ) reaction is sufficiently high to drive the recoiling Ge atom into the interstitial position [62]. The dopant atom in interstitial positions cannot contribute to the total number of carrier concentration [63]. Thus, defects created during the irradiation can significantly affect the performance of the sensor at low temperature. It should be mentioned that defect formation may depend on irradiation conditions since both the flux and energy of fast neutrons are responsible factors. The performance of NTD Ge sensors over a wide range of carrier concentration 3 x $10^{14}/\text{cm}^3$ to 1.8 x $10^{17}/\text{cm}^3$ was studied in detail by Itoh *et al.* [29]. Generally high

temperature annealing is employed to cure the crystal defects and annealing conditions need to be optimized depending on the defect type and the density.

Kuriyama *et al.* [64] had reported the recovery of damages in a neutron irradiated Ge wafers as a function of annealing temperature for a hole concentration of 3.5 x $10^{14}/cm^3$. Figure 3.1 shows Rutherford Back Scattering

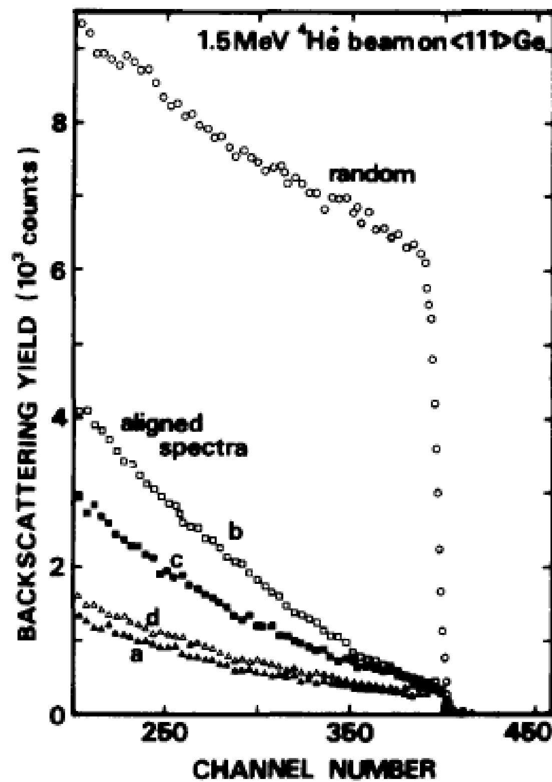

Figure 3.1: Back scattering spectra for 1.5 MeV $^4He^+$ along $< 111 >$ channeling/random direction in a neutron irradiated germanium for various annealing stages: (a) Unirradiated (n-type) (b) Irradiated-before annealing (c) annealed at 300°C (d) annealed at 600°C. Figure from [64].

(RBS) yield for 1.5 MeV $^4He^+$ along $< 111 >$ channeling/random direction for Ge samples at various stages. It is clear from the figure 3.1 that RBS yield of the irradiated sample annealed at 600°C for 30 min in the Ar gas is close to the unirradiated sample. Pasca *et al.* [38] have employed annealing at 400° C for 6 hours for carrier concentration in the range of 5 – 7 x $10^{16}/cm^3$. Palaio *et al.* [65] have also discussed effects of thermal annealing in the Ar gas and have reported that annealing at higher temperatures (500° C) resulted in contamination of samples due to rapidly diffusing impurities. They further observed that the NTD Ge samples left at ambient temperature for eight months after irradiation showed improvements similar to thermal annealing. This is desirable for rare decay studies as annealing can introduce trace impurities in the sensors.

A systematic study of the fast neutron induced damage in the NTD Ge samples for neutron fluence in the range of 2 x $10^{18}/cm^2$ to 1.4 x $10^{19}/cm^2$ which corresponds to the carrier concentration of (0.5 - 3.3) x $10^{17}/cm^3$ is studied [66]. In the present case, the thermal neutron flux covered a higher range than the reported values in Ref. [64]. Hence, the annealing was done for a longer duration, namely, at 600° C for 2 hours. Samples were annealed in the vacuum sealed quartz tube to avoid contamination. Positron Annihilation Lifetime Spectroscopy (PALS) and Channeling have been employed

for studying fast neutron induced defects before and after annealing. Details of these measurements are presented in this chapter.

3.1 NTD Ge Surface Studies by SEM-EDAX

The irradiated Ge wafers were studied for its surface contamination using SEM (Scanning Electron Microscope) - EDAX (Energy Dispersive X-ray Analysis) technique. Samples (a) without any treatment, (b) cleaned with Isopropyl alcohol, (c) cleaned with HF, (d) annealed at 400° C for 6 hours in Ar atm, (e) annealed at 600° C for 2 hours in Ar atm and (f) annealed at 600° C for 2 hours in a vacuum sealed quartz tube were taken for the studies. Figure 3.2 shows the SEM image of the NTD Ge samples at various stages. From the figure, one can infer that the samples before annealing contain mainly surface oxides. Sample cleaned with isopropyl alcohol did not show any improvement, whereas HF cleaning had tremendously reduced the Oxygen content. A few micron size patches are clearly visible in the samples annealed in Ar atmosphere. The EDAX study showed some of these patches to be rich in O, Ca, Mg, Al, Si, Cl and K. This might be due to the surrounding environment during annealing. One could observe that the sample annealed in vacuum sealed quartz tube and cleaned with isopropyl alcohol shows minimal surface contamination in the SEM. The study shows that HF cleaning and annealing in vacuum sealed quartz tube results

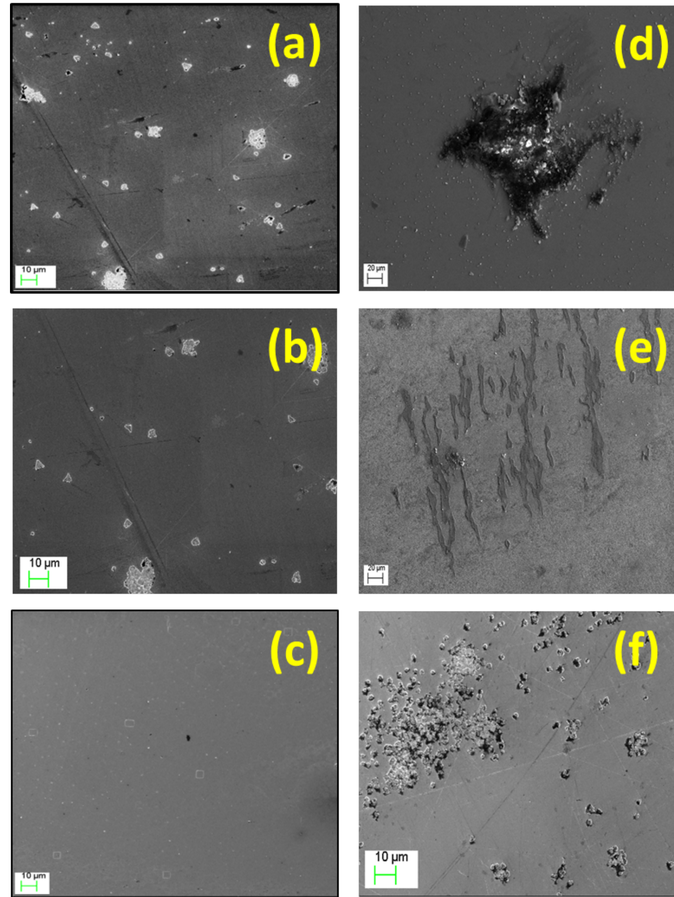

Figure 3.2: SEM images of NTD Ge (a) Uncleaned (b) Cleaned with isopropyl alcohol (c) Cleaned with HF (d) Annealed at 400° C for 6 hours in Ar atm (e) Annealed at 600° C for 2 hours in Ar atm (f) Annealed at 600° C for 2 hours in a vacuum sealed quartz tube and cleaned with isopropyl alcohol.

in minimal surface contamination. Thus, the irradiated samples annealed in vacuum sealed quartz tube and then cleaned with HF are preferred.

3.2 Positron Annihilation Lifetime Spectroscopy

Positron Annihilation Lifetime Spectroscopy (PALS) qualifies the type of defects through the positron lifetime measurement. In this technique, a positron is made to incident on the sample. During the interaction the positron experiences both attractive (due to electrons) and repulsive (due to core ions) forces. In a defect free crystal, the positron interacts with valance electrons and annihilates to give two 511keV gamma rays and the measured lifetime corresponds to the bulk lifetime. On the other hand, when a positron interacts inside a crystal with defects, it is more likely to stay in the defect due to the repulsive force of ions and consequently its lifetime increases. Positron lifetime increases with the defect size. In an experiment to study the correlation between positron annihilation features and lattice defects, G. Fabri et al., [67] had measured the lifetime of positron as 380$\pm$50 ps in a Ge sample irradiated with a neutron fluence of about 2 $\times 10^{18}/\mathrm{cm}^2$, which is much larger than the bulk lifetime of positron (240$\pm$50 ps). Details of PALS employed in the current work are given as follows.

3.2.1 PALS Experimental Details

For PALS measurement a ^{22}Na ($\sim$ 8 μCi) source, covered with Kapton foil, was sandwiched within two identical (virgin/irradiated) Ge samples and mounted between two plastic scintillators kept at 180° w.r.t. each other.

The β^+ lifetime was obtained from Time to Amplitude Converter (TAC) spectrum with a 1.27 MeV γ-ray as a start signal and the 511 keV γ-ray as a stop signal. The time resolution measured with ^{60}Co source was 262 ps and the ADC calibration constant was 12.5 ps/channel. The lifetime spectrum was analysed using PATFIT program [68]. Figure 3.3 shows the schematic view of the experimental setup of PALS and figure 3.4 shows the decay scheme of positron source ^{22}Na.

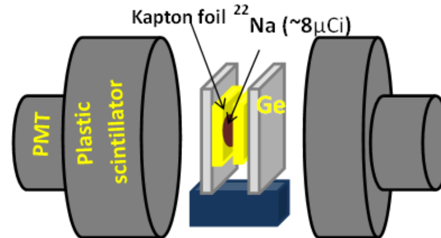

Figure 3.3: Schematic view of the PALS set up.

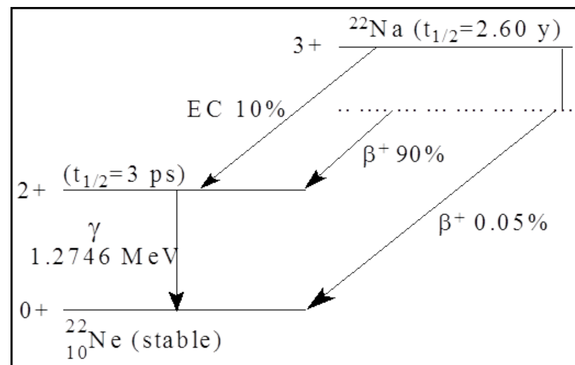

Figure 3.4: Decay scheme of a ^{22}Na nucleus.

3.2.2 PALS Results

Figure 3.5 shows PALS decay spectra of NTD Ge B, before (red) and after (black) annealing. It is clearly seen from the figure 3.5 that annealed samples decay faster than the unannealed samples.

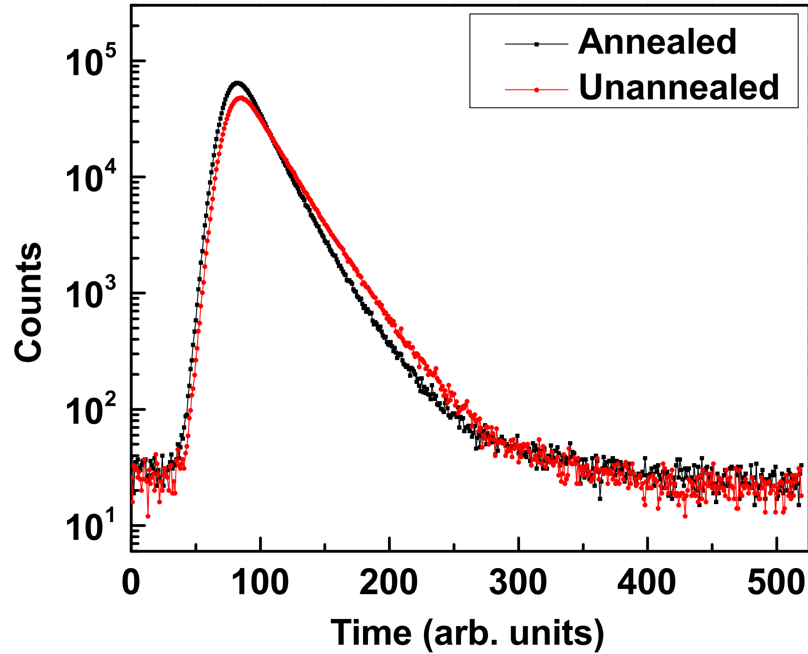

Figure 3.5: PALS spectra of NTD Ge B, before (red) and after (black) annealing. Positron in annealed samples decays faster than the unannealed samples.

The PALS results of the virgin, irradiated samples before and after annealing are tabulated in Table 3.1. The measured lifetime of positron (τ_{β^+}) for both $< 100 >$ and $< 111 >$ virgin samples is consistent with that of the bulk Ge crystal ($\tau_{\beta^+} = 228$ ps). The measured positron lifetime $\tau_{\beta^+} \sim 293.6$ ps

Table 3.1: Measured positron lifetime (τ_{β^+}) in NTD Ge using PALS.

Samples		τ_{β^+} (ps)	τ_{β^+} [69] (ps)
virgin $< 111 >$		227.8 ± 0.3	228(Bulk)
virgin $< 100 >$		232.0 ± 0.3	228(Bulk)
B	before annealing	293.6 ± 0.4	293(Monovacancy)
	after annealing	225.6 ± 0.3	228(Bulk)
D	before annealing	294.0 ± 0.3	293(Monovacancy)
		401 ± 30	401(Vacancy clusters)
	after annealing	233.0 ± 0.4	228(Bulk)
E	before annealing	293.5 ± 0.4	293(Monovacancy)
	after annealing	228.0 ± 0.4	228(Bulk)
F	before annealing	294.0 ± 0.6	293(Monovacancy)

in all the irradiated samples before annealing, indicates that defects are of 'monovacancy' type. The intensity of the τ_{β^+} lifetime were 100% for all the samples except for the sample D, where two lifetime components corresponding to monovacancy (Intensity $\sim 90.0 \pm 2.5$ %) and vacancy cluster (Intensity $\sim 9.4 \pm 2.4$ %) were observed [70]. The observed single lifetime implies that β^+ has undergone saturation trapping. Hence, the exact defect concentration can not be inferred and is estimated to be greater than 0.1 %. The τ_{β^+} observed for all the annealed samples is very similar to that of the virgin crystal indicating complete recovery of defects.

3.3 Channeling

In a single crystal, when charged particle is incident along the axial or planar directions, the trajectory is restricted to open channels between

planes/rows due to a series of small angle collisions. This is known as channeling and it is strongly directional. In a perfect crystal lattice structure, any close impact parameter process like RBS is reduced. The presence of defects in crystal disturbs the periodicity of the potential and thereby enhances the RBS yield. Thus, crystal channeling is found to be a sensitive tool for probing defects [71] and has been extensively used for studying the variety of materials. As mentioned earlier, the defects in the irradiated samples are probed with channeling and an estimation on the defect density (N_D) can be obtained from increase in the minimum yield for RBS along channeled direction as

$$N_D = N\left[\frac{\chi_{min}^{irr} - \chi_{min}^{o}}{1 - \chi_{min}^{o}}\right] \tag{3.1}$$

where N is the number density of Ge atoms, χ_{min}^{irr} is the χ_{min} of the irradiated sample and χ_{min}^{o} is that of virgin sample [72]. In the channeling experiment, the χ_{min} = Yield (channelled)/Yield (random) is obtained by taking the yield for about 100 keV (corresponding to a depth of 316 nm) below the surface peak of the channelled spectrum, as higher RBS yield at surface peak shows the imperfection in the first monolayer of atoms in the crystal. The details of channeling studies in NTD Ge are given below.

3.3.1 Channeling Experimental Setup

The channeling experiment with 2 MeV alpha particles has been carried out using Pelletron Accelerator RBS-AMS Systems (PARAS) facility at Inter University Accelerator Centre (IUAC), New Delhi [73]. The schematic

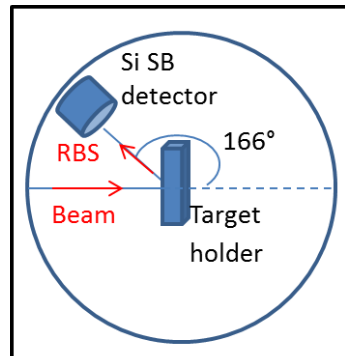

Figure 3.6: Schematic view of channeling setup.

view of the channeling experiment is shown in Figure 3.6. The samples

Figure 3.7: Samples placed on channeling sample holder.

were glued to the sample holder with double sided carbon tape (Figure 3.7).

Rutherford backscattering was measured at a θ_{lab} = 166° with a silicon surface barrier detector. The beam current on the sample was maintained below 5 nA throughout the measurement to minimize damage to the sample. Initially, a detailed scan was carried out with 20nC/cell to locate the axis. Later the sampling spot of the sample was changed to do the actual measurement. In this way the defects produced during axial scan was avoided in the actual data collection. In the fresh spot, a quick scan was done to confirm the axis with 100nC/cell and the channeling spectra was acquired for a charge of 5 μC. Each channeling spectra was continued with a random spectrum for a charge of 2 μC to check the consistency in the measurement. Figures 3.8 and 3.9 show 2D scan and axial scan of both $< 111 >$ and $< 100 >$ crystal, respectively. The 2D scan shows the depth resolving structural information in the scale of 0 to 1. The axial dip of both irradiated $< 111 >$ and $< 100 >$

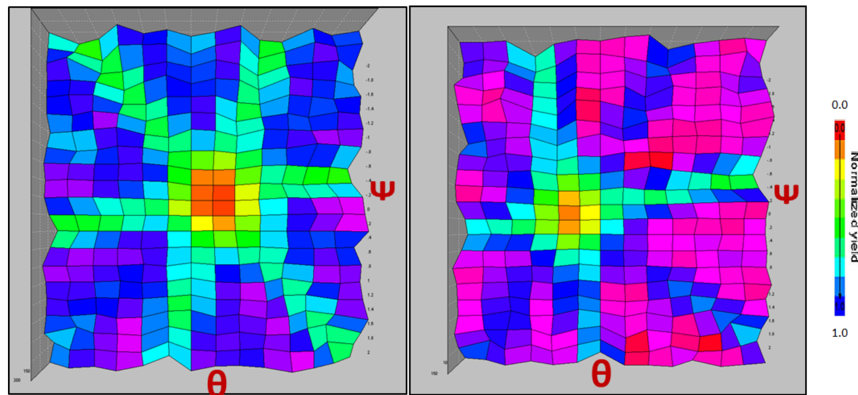

Figure 3.8: 2D channeling spectra of $< 111 >$ (left) and $< 100 >$ (right) Ge crystal. Depth resolving structural information is given in a scale of 0 to 1.

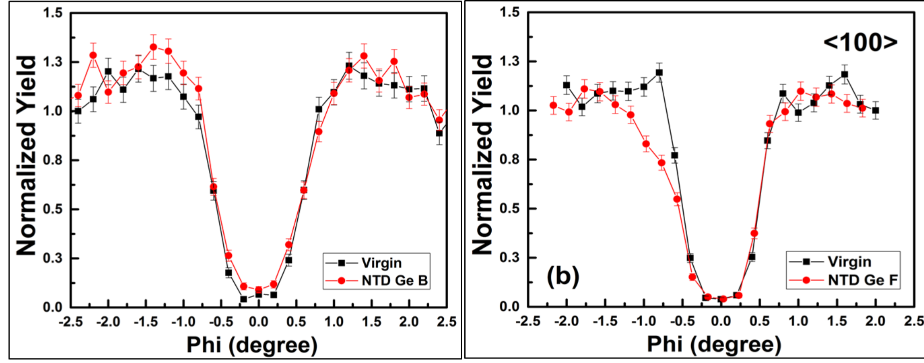

Figure 3.9: Axial dip of NTD Ge crystal $<111>$(left) and $<100>$(right).

Ge crystal did not show a significant change from that of the virgin Ge crystal. Left side of axial dip of the sample NTD Ge F $<100>$ shows the planar effect.

3.3.2 Channeling Results

Figure 3.9 shows that the minimum yield (χ_{min}) in NTD Ge B (0.09 ± 0.02) is higher compared to that for the virgin sample ($\chi_{min} = 0.06 \pm 0.02$). It is also evident that the measured half angle $0.55° \pm 0.05°$ is similar for both the samples. No measurable changes in the width of the channeling dip were observed for any of the samples. Figure 3.10 also shows the channeled spectra for the sample B after annealing along with the virgin $<111>$ sample. It is evident that the channeling effect observed in the annealed sample B is somewhat better than the virgin sample, implying complete recovery of damages. It was found that the RBS spectra of samples E and F irradiated

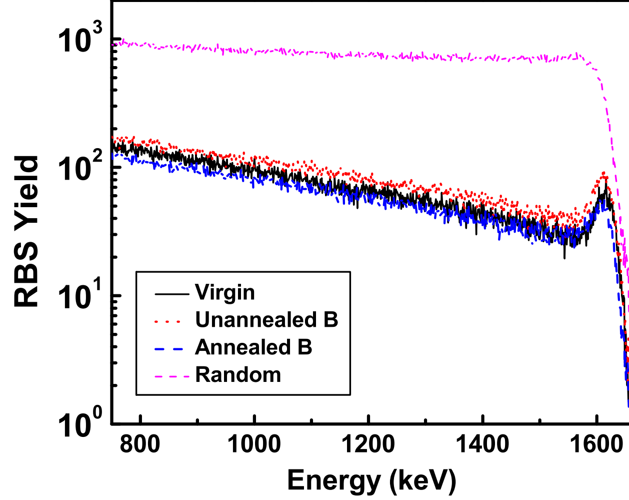

Figure 3.10: The RBS spectra along $< 111 >$ axis of the unannealed and annealed Sample B along with the virgin sample. The spectrum in the random orientation is also shown for comparison.

with lower neutron fluence ($N_{fast} < 4 \times 10^{16}$ n/cm^2) were very similar to that of the virgin sample. However for the higher neutron fluences, i.e. in sample D (see Figure 3.11) and sample B, increase in the RBS yield of the channeled spectra was observed.

It should be mentioned that unannealed samples showed the presence of defects even after four months since irradiation. Thus unlike in Ref. [65], for neutron fluences $> 10^{17}/\mathrm{cm}^2$ studied in the present work leaving the samples at ambient temperature is not sufficient and high temperature annealing was essential. The estimated defect densities from equation 3.1 for samples B and D, where a measurable change in χ_{min} was observed for unannealed samples with respect to virgin samples are tabulated in Table 3.2. The de-

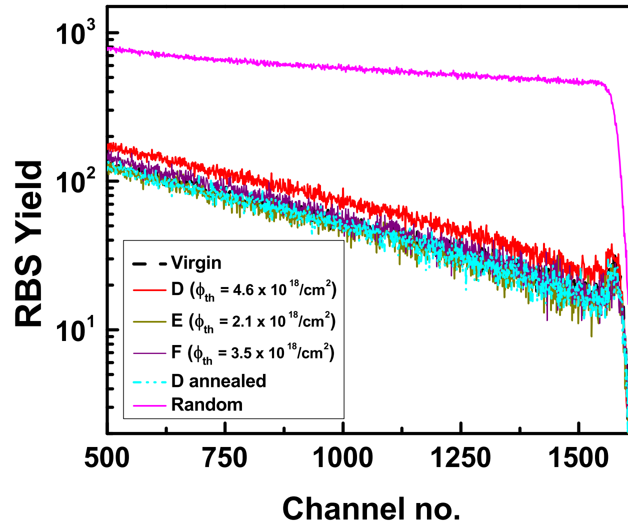

Figure 3.11: The RBS spectra along < 100 > axis of the samples D, E, F and annealed D together with that of the virgin sample. The spectrum in the random orientation is also shown for comparison.

fect concentration from the channeling experiment is estimated to be 1.6 % and is consistent with PALS measurement (> 0.1 %). It may be added that the estimated N_D values for 50 keV and 100 keV energy window below the surface peak defined depth are similar within error, indicating no significant dechanneling effects in the near surface region.

Table 3.2: Estimated χ_{min} and N_D of virgin and irradiated samples from the channeling data. Defect densities could not be estimated for samples with very low defects and the corresponding data space are left blank.

Samples		χ_{min} (%)	N_D x 10^{20} cm^3
virgin $< 111 >$		4.44 ± 0.08	-
virgin $< 100 >$		4.19 ± 0.05	-
B	before annealing	5.92 ± 0.06	(6.8 ± 0.4)
	after annealing	3.22 ± 0.09	-
D	before annealing	5.76 ± 0.06	(7.3 ± 0.4)
	after annealing	3.68 ± 0.13	-
E	before annealing	3.49 ± 0.12	-
	after annealing	3.29 ± 0.12	-
F	before annealing	3.90 ± 0.13	-
	after annealing	3.96 ± 0.13	-

3.4 Summary

Fast neutron induced defects have been studied using PALS and Channeling. The PALS measurements indicated monovacant type defects for all irradiated samples, whereas the channeling studies revealed no significant defects for fast neutron fluence upto $\sim$ 4 x $10^{16}/cm^2$. These fast neutron induced defects were observed in the irradiated samples even after about 4 - 8 months of irradiation. It is shown that vacuum annealing at 600 °C for $\sim$ 2 hours is sufficient to recover the damage in the irradiated samples, as verified from both PALS and Channeling.

Chapter 4

Characterization of NTD Ge sensors

Carrier concentration measurement and low temperature resistance measurement were carried out on the NTD Ge samples, fabricated from the irradiated Ge wafers. Apart from the characteristic studies, this chapter also explains the cryo setup fabricated to do resistivity measurement of a sample from 4K to 300K and to check the stability of the electrical contacts over various thermal cycles. In addition, this chapter contains the details of the Labview program developed for the data acquisition.

4.1 Fabrication of NTD Ge

After a cool-down period of 45 days post n-irradiation, the Ge samples were taken out and cut into several smaller pieces for further studies. The samples were then annealed at 600° C for 2 hours in a vacuum sealed quartz tube to anneal the irradiation induced damages. The annealed Ge

wafers were cleaned with HF before the fabrication of NTD Ge sensors. Au(88%)–Ge(12%) of about 50 nm thickness contact pads were sputtered on the HF cleaned oxygen free NTD Ge surface and rapid thermally annealed at 400° C for 2 min. Electrical connections to the sample were made by wedge bonding Al/Au wires (ϕ = 25 μm) to the Au-Ge contact pad and to the sample mount.

4.2 Carrier concentration measurement

As already explained in chapter 1, highly sensitive NTD Ge sensors can be produced by doping Ge below the metal insulator transition (MIT) regime. The carrier concentration produced by doping can be estimated from the production rate (Table 2.2) and the neutron fluence computed from the reactor data. The same can be verified experimentally by Hall effect measurement. The experimental details of Hall effect measurements are described in the following sections.

4.2.1 Experimental details

Carrier concentrations in annealed samples were estimated from the Hall effect measurement carried out using Van der Pauw method on a 7 x 4 mm^2 symmetrical sample. Figure 4.1 shows a picture of the contact pattern. The Hall voltages were measured at 77 K and at 300 K with 100 μA current

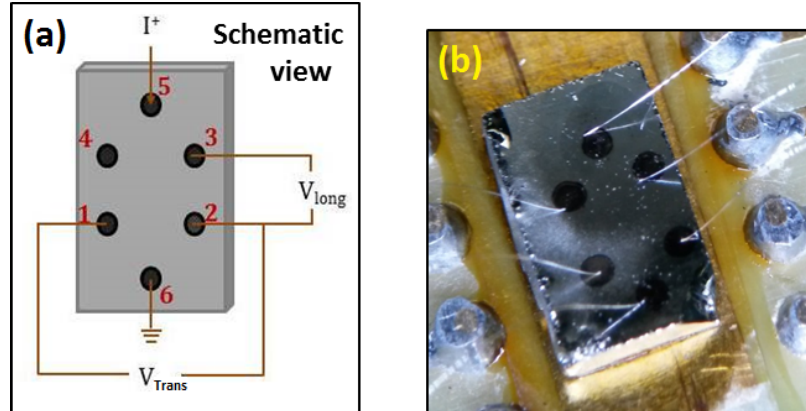

Figure 4.1: (a)Schematic diagram of the V-I measurement. (b) A picture of the NTD Ge sample with contacts pads for Hall effect measurement by Van der Pauw method.

and in a magnetic field varied between –1 to 1 Tesla. The voltages V_{Trans} (transverse voltage) and V_{long} (longitudinal) were measured simultaneously with two lock-in amplifiers (Figure 4.2). This enabled the correction for the

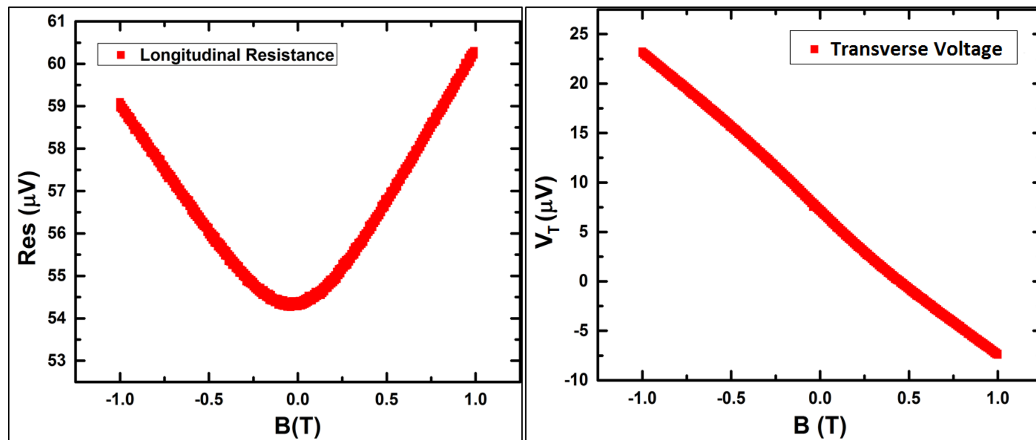

Figure 4.2: Longitudinal resistance (left), Transverse voltage (right) of NTD Ge sample I at 77K.

magneto-resistance effect due to lack of parallelism in connections, thereby allowing unambiguous estimation of the Hall coefficient and the carrier concentration (N_c).

4.2.2 Results and discussions

The observed transverse voltage (V_T), in general, comprises Hall voltage (V_H), admixture (β) of resistive voltage drop (V_R) due to geometric misalignment and measurement offset (V_{offset}).

$$V_T = V_H + \beta.V_R + V_{offset} \tag{4.1}$$

in the above equation V_H changes sign with respect to the applied magnetic field (B) whereas the term due to magnetoresistance and measurement offset are independent of the sign of the magnetic field.

$$V_H(B) = -V_H(-B) \tag{4.2}$$

$$V_R(B) = V_R(-B) \tag{4.3}$$

The Hall voltage is extracted as

$$V_H = [V_T(+B) - V_T(-B)]/2 \tag{4.4}$$

A typical plot of the extracted Hall voltage (V_H) is shown in figure 4.3. These voltages were fitted to a straight line and the slope (V_H/B) is used to

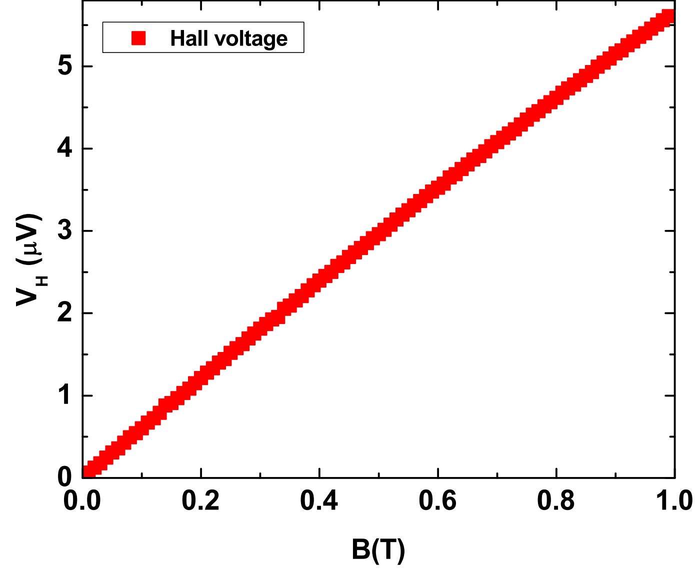

Figure 4.3: Extracted Hall voltage of the sample NTD Ge I at 77 K.

estimate the carrier concentration (n) by the following expression.

$$n = \left[\frac{B.I}{e.V_H.t} \right] \tag{4.5}$$

where e is the electric charge, I is the supplied current and t is the thickness of the sample.

The estimated carrier concentration at 77 K and 300 K are tabulated in Table 4.1. The carrier concentrations expected from the neutron fluence, which in turn are derived from the reactor power, are also listed in Table 4.1. For NTD Ge, both holes and electrons participate in the electrical conduction. Hence, mobilities of both the carriers contribute to the Hall coefficient and is given by,

$$R = \frac{\mu_n^2 p - \mu_e^2 n}{2(\mu_n p + \mu_e n)^2} \tag{4.6}$$

Table 4.1: The carrier concentrations of NTD Ge from Hall effect measurement at 77 K and 300 K along with expected carrier concentrations obtained from the given neutron fluence.

Sample	Carrier concentrations ($\times 10^{16}$cm^{-3})					
	Hall Measurement		From neutron fluence			
	77K*	300K*	^{71}Ga	^{75}As	^{77}Se	†Net carrier concentration
B	34.20	38.90	45.16	10.89	0.67	32.93
C	21.10	26.00	29.45	7.10	0.44	21.47
D	11.10	21.3	23.20	5.53	0.35	17.00
E	4.45	7.25	7.00	1.66	0.11	5.12
I	4.17	4.87	5.97	1.42	0.09	4.37

* Errors are within 0.1 %.
† Net carrier concentration = ^{71}Ga - (^{75}As + 2 $\times$ ^{77}Se).

As explained by Morin [74] carrier concentration estimated at 77 K, where the Hall factor is close to unity, should be used for comparison with values calculated from the neutron fluence and is plotted in Figure 4.4. It can be seen from the Figure 4.4 that the carrier concentration obtained from the Hall effect measurement at 77 K and the neutron fluence shows good correlation. Data for samples F and G are also shown to indicate the complete range. In the present data for $< 100 >$ samples Hall factor at 300 K was found to be vary in the range 1.2 to 1.9 (value reported in Ref. [74] is 1.8), while $< 111 >$ samples (B and C) show a much smaller value close to ~ 1.2.

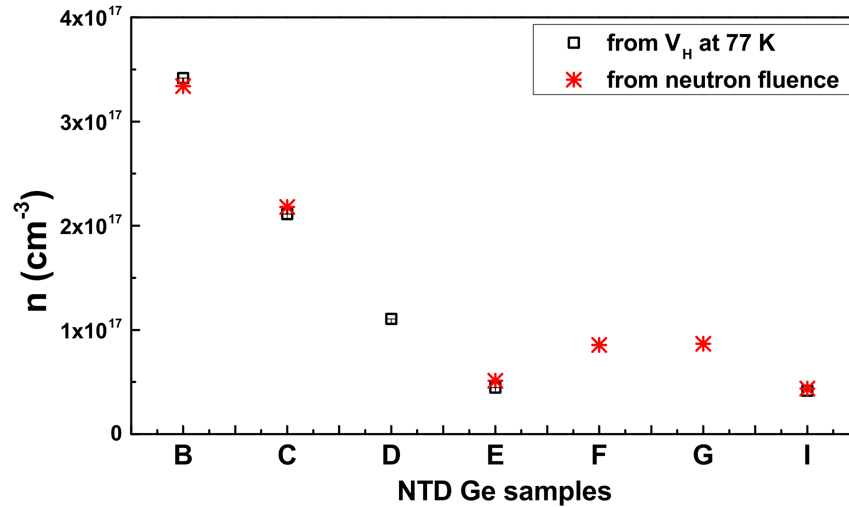

Figure 4.4: Comparison of the carrier concentration estimated using Hall Effect measurement at 77K and estimated from the reactor power data.

4.3 Low temperature measurement

The NTD Ge samples of known carrier concentration were taken down to mK to observe its resistance behaviour. The stability of the contacts on NTD Ge was tested with the cryo insert, in various thermal cycles before mounting for resistance measurement. Labview data acquisition system were developed to perform the resistance measurement with the commercial AVS resistance bridge. This resistance bridge restricts the resistance measurement to the maximum of 2 MΩ. Hence, a dedicated measurement system with an ultra low current source and ultra high input impedance voltage amplifier along with the Labview signal express were used for measuring

higher resistance. The description of the measurement system is given in detail in the following sections.

4.3.1 4K Cryoinsert for resistivity measurements between 4 to 300 K

For designing a bolometer, it is essential to understand thermal properties of the different material which will be used for making links, mounts etc. The dilution refrigerator cannot be used for measurements above 1 K. In order to study the thermal properties of a sample over a wide range of temperature (4 to 300 K), a separate insert which fits into a standard LHe dewar has been constructed. The resistivity insert consists of outer SS tube (OD of 34 mm; ID of 30.49 mm; Length of 145 cm), which serves as IVC (Inner Vacuum Chamber) for the measurement. The schematic of the insert is shown in Figure 4.5 and 4.6. Inner insert consists of five parts, namely, Fischer connector welded with hollow SS pipe, followed by SS tube, Teflon and finally a copper rod. A total of eight 3 mm holes is provided in the inner part of the insert for the wiring connection. Teflon is used as a thermal insulation for the copper rod (to shield it from room temperature). On the copper rod, a flattened surface is provided for sample mounting and adequate space is left for winding a heater wire (manganin). Eight manganin wires are used for doing four probe resistive measurement of sample and sensor, whereas two copper leads are used for the heater. The Cerenox sensor was mounted

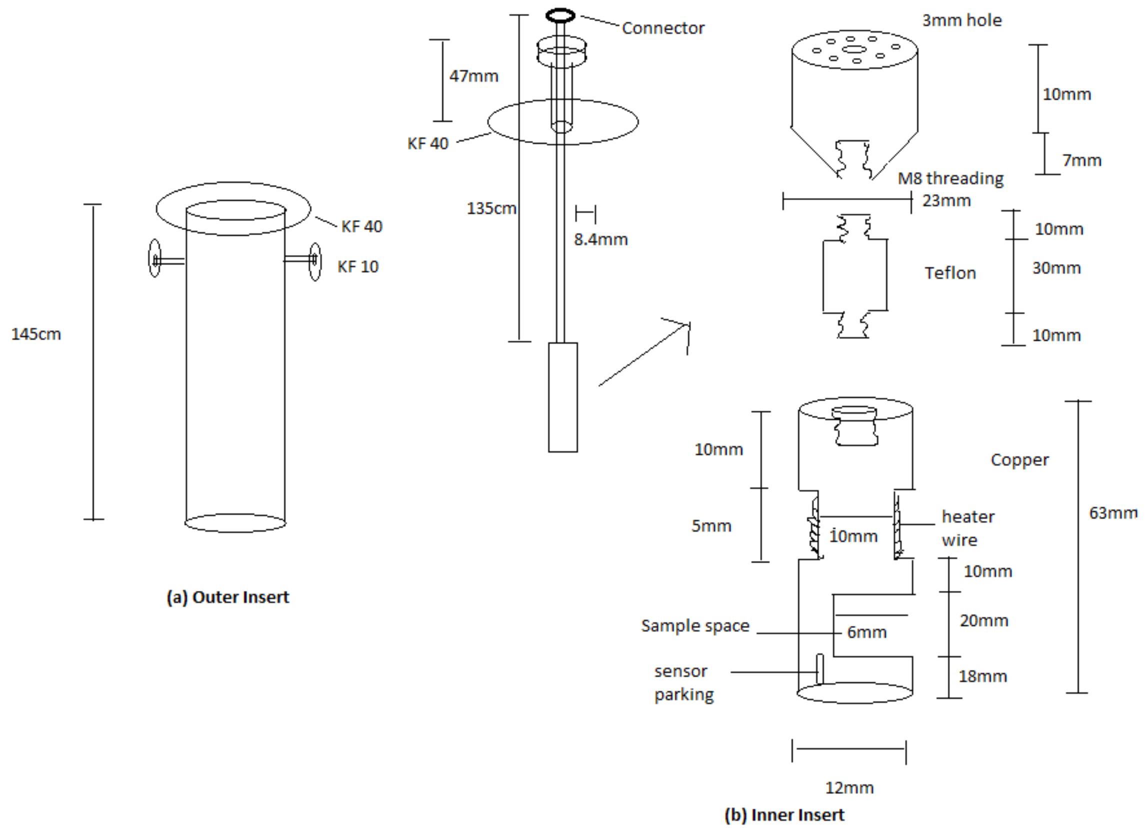

Figure 4.5: Schematic view of 4K Cryoinsert.

at the end of the copper rod. Radiation baffles are added in the inner insert to minimize thermal radiation. The insert has been tested in LN_2 bath and in LHe bath (Figure 4.6). The calibration of the cerenox sensor has been checked with the known superconductors (like Nb, NbTi, Ta) using SQUID measurement. The stability of the contacts on the NTD Ge surface was examined several times in this insert, before doing the resistance measurement in the dilution refrigerator.

Figure 4.6: 4K Cryoinsert setup for resistivity measurements.

4.3.2 PID control and development of DAQ

To carry out resistivity or specific heat measurement at a particular cryogenic temperature, the system needs to be stabilized at a temperature. The system is generally controlled by a temperature controller, either in an open loop or closed loop mode. In an open loop mode, the heater power can be applied manually to raise and stabilize the temperature of the system. In a closed loop mode, the system can operate automatically with the suitable PID control. The Proportional, Integral, and Derivative feedback control involves setting a gain (P) of the heater power, quiescent (I) of heater power and rate (D) of stabilization of the system. Figure 4.7 shows the nature of the system when only P, P+I and P+I+D are applied. The PID values have been optimized for the 4 K insert.

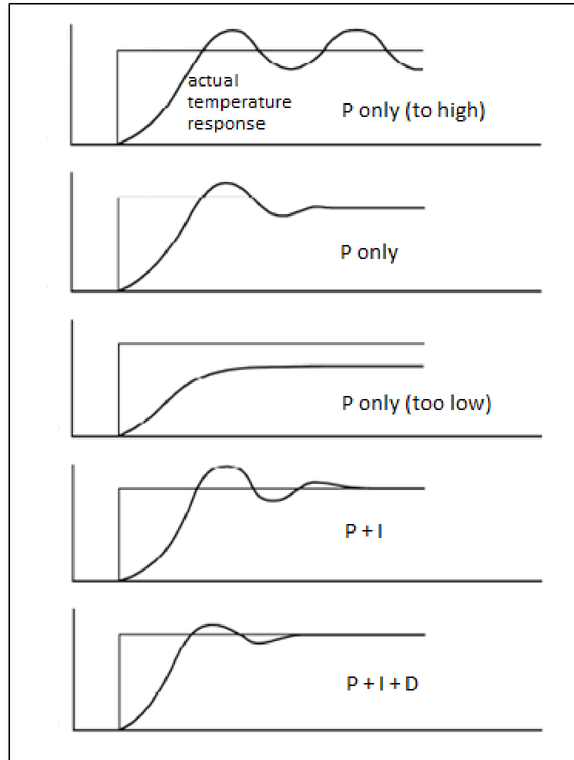

Figure 4.7: System responding for proportional, integral and derivative values.

Labview data acquisition has been developed in such a way that the system can work in either closed loop or open loop mode. Figure 4.8 shows the block diagram of a closed loop mode where the feedback control and the PID sub Virtual Instruments are used. Figure 4.9 shows the front panel of the Labview program where the resistance measurement can be done in the given range and in the given stability in fine steps. The commercial resistance bridge can measure the resistance of maximum 2 MΩ. Resistance higher than 2 MΩ was measured using NI-PXI 6229 card along with the

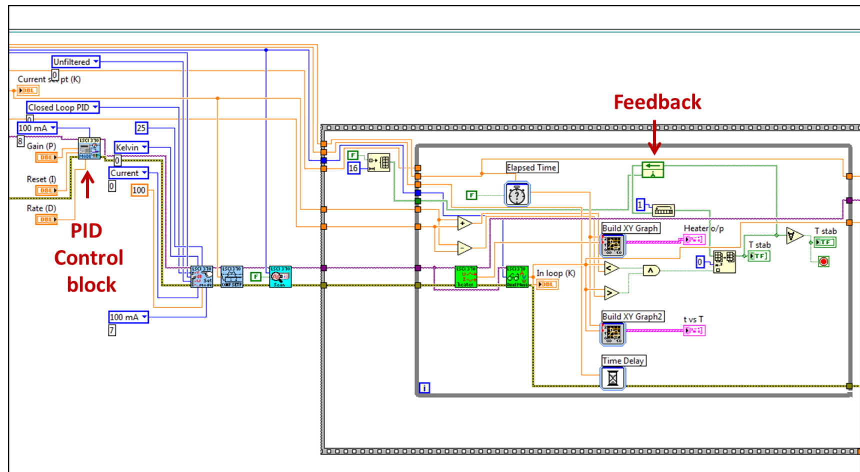

Figure 4.8: Block diagram of the Labview program with feedback control.

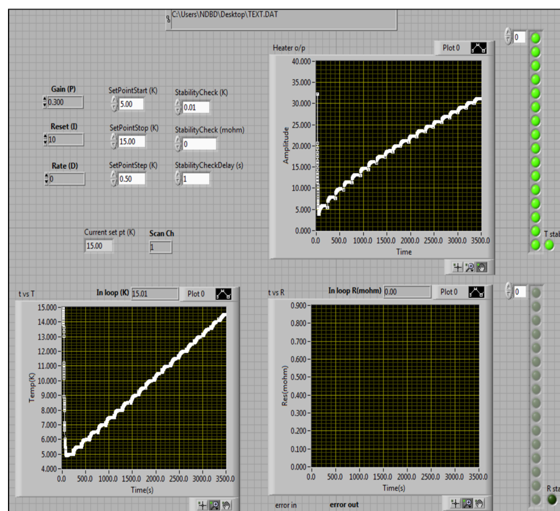

Figure 4.9: Front Panel of the Labview program with feedback control.

Labview signal express to communicate with the current source and the voltage amplifier. The schematic sketch of DAQ using AVS resistance bridge and NI-PXI 6229 are shown in Figures 4.10 and 4.11, respectively. The current source was a Voltage to a Current converter with an output adjustment range of ±1000 pA (CSE09NVG from RDM-Apps). The reference

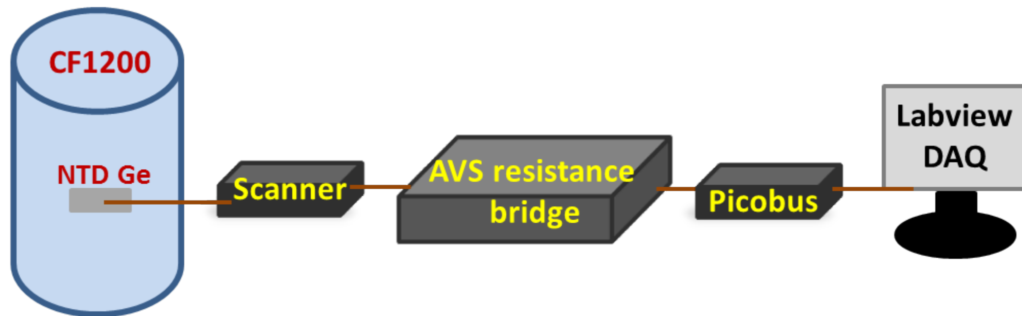

Figure 4.10: Schematic sketch of the AVS measurement system.

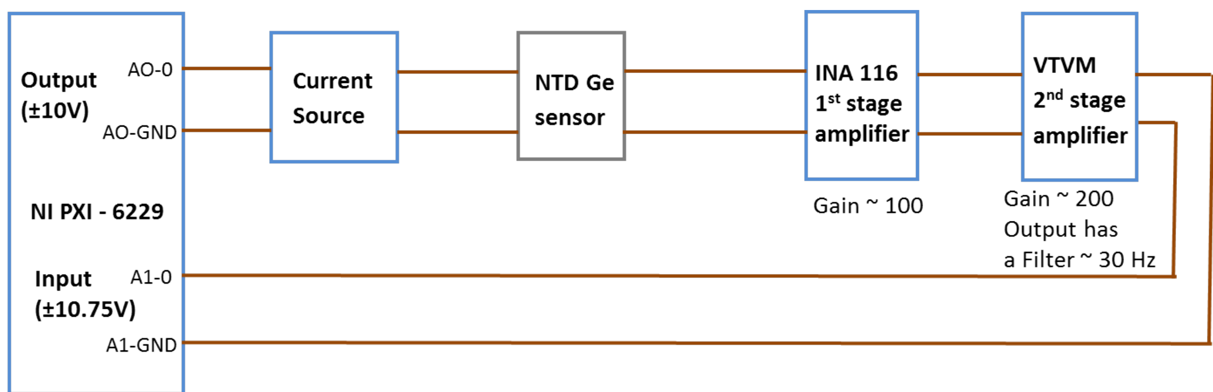

Figure 4.11: Schematic sketch of the NI measurement system.

voltage to the current source is supplied by an analog output channel of NI-PXI 6229 (16 bit DAC). The first stage voltage amplifier INA116 (from TEXAS instruments) with an input impedance of greater than $10^{15}\Omega$ and a gain of 100 was used. The second stage voltage amplifier module (VTVM from RDM-Apps) with a gain of 200 was used in the measurement system when required.

4.3.3 Resistance measurement of NTD Ge at mK

Low temperature resistance measurements of the NTD Ge samples were carried out in a high cooling power (1.4 mW at 120 mK) cryogen free dilution refrigerator (CFDR) setup at TIFR, Mumbai [75] using a four probe technique. All connecting wires below 4K station were superconducting (NbTi/Al) to minimize the heat load.

Experimental details

NTD Ge samples were fabricated with two/six contact pads on the same side of the Ge wafer (refer Figure 4.1). The samples were initially mounted on the G-10 substrate coupled with the Cu base via Teflon. The saturation in the resistance of the NTD Ge sensor was observed at around 75 mK. This showed that teflon could not provide enough thermal conductivity to cool down the sample assembly. The thermal conductivity was improved by replacing the Teflon coupling by Cu. Finally, saturation due to Kapitza resistance [76] was overcome by mounting the NTD Ge samples directly on the Cu platform with a thin insulating layer, as showing in Figure 4.12. The saturation of resistance was not seen till 25 mK. The various sample mount are shown in Figure 4.13. The sensor performance in T = 10 to 400 mK

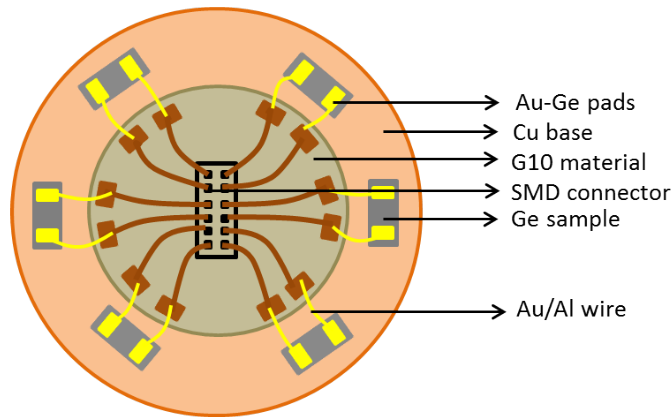

Figure 4.12: Schematic view of sample mount.

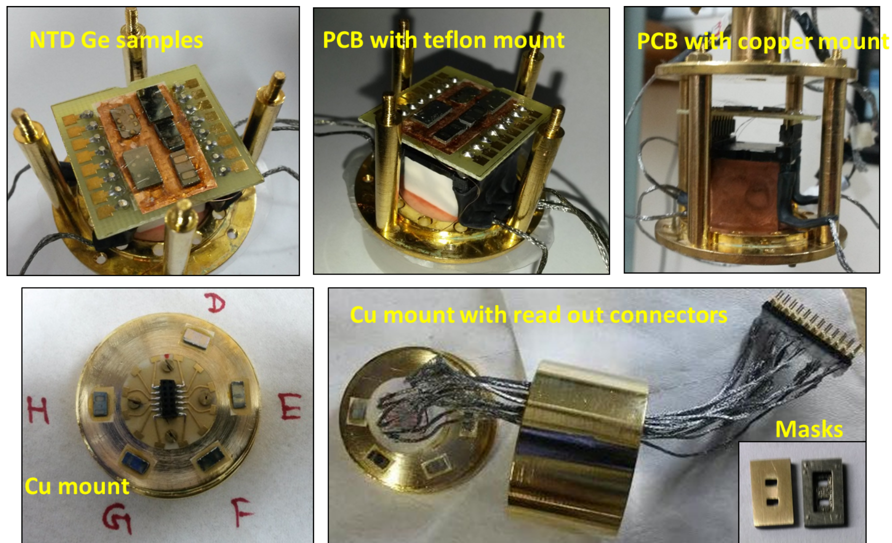

Figure 4.13: Evolution of sample mount for better thermal conductivity.

were measured using a commercial resistance bridge AVS-47B with a dedicated Labview interface and with NI-PXI with Labview signal express, specially developed for this setup. To avoid the self heating of the sensor during measurement, the net power dissipated in the sensor was maintained below 10 fW.

The output voltage was recorded by supplying current at periodic intervals. The recorded data of a single pulse (on and off of input current) by Labview signal express is shown in Figure 4.14. The data show a dou-

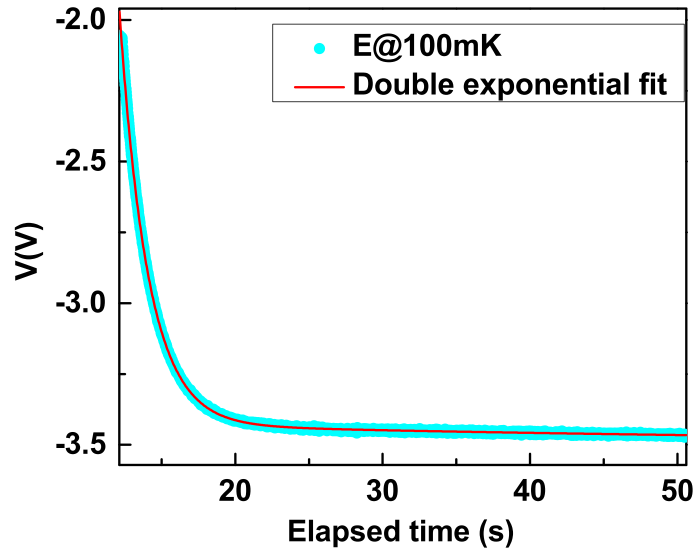

Figure 4.14: Measured voltage with respect to elapsed time.

ble exponential decay indicating “lumped τ_2 effect” [77], arising due to the presence of multiple thermal pathways. Data were fitted by double exponential decay and the voltages were extracted for the corresponding applied current. The VI characteristics of the obtained NTD Ge sample F at 200 mK is plotted in Figure 4.15. For a sample with the ohmic contact, one would expect a linear VI characteristics. But, most of the samples below 400 mK

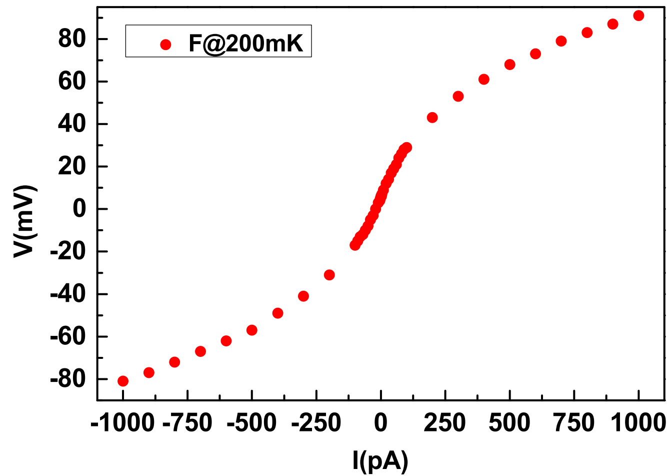

Figure 4.15: VI characteristics of NTD Ge F at 200 mK.

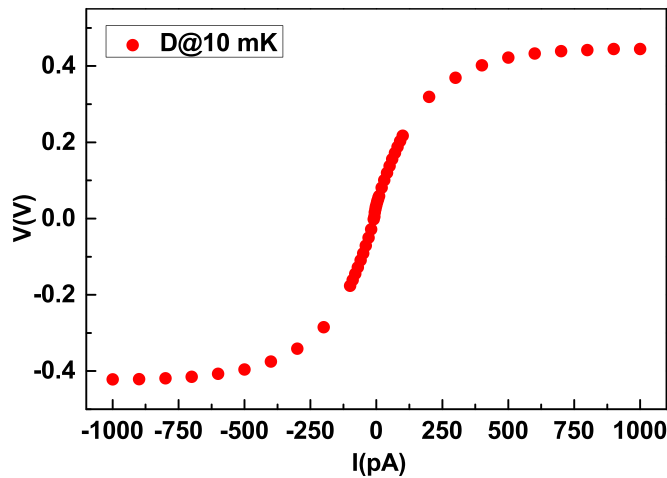

Figure 4.16: VI of characteristics NTD Ge D at 10 mK.

show a Schottky diode like behaviour. The Schottky barrier, as measured is extremely small ($\sim$ mV) and present only at the lowest temperature.

The resistance measurement of the lowest dose sample H at lower temperature is limited by the current source (less than 2 pA is not possible in the

measurement system), whereas the highest dose sample D at higher temperature is limited by the voltage amplifier and the noise in the measurement. Figure 4.16 shows the highest neutron dose sample D (among $< 100 >$ samples) at the lowest possible temperature 10 mK. The lowest neutron dose sample H was tested for its diode behaviour at the highest possible temperature in the dilution refrigerator. Temperature of 724 mK was achieved by collecting ^{3}He into the dump and allowing only ^{4}He in the circulation line. The sample showed perfect ohmic nature (Figure 4.17) at this temperature. This suggests that at higher temperature the sample overcome the Schottky

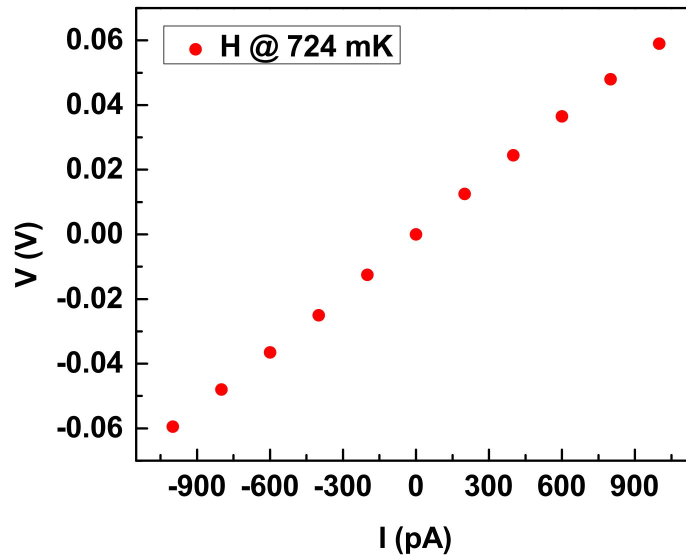

Figure 4.17: VI characteristics of NTD Ge H at 724 mK.

barrier. It is observed that the sample E shows ohmic characteristics at all temperature. This suggests that the electrical contacts in samples other than

E can be improved. There are several electrical interfaces from sample to the readout system, such as NTD Ge to Au-Ge pad, Al/Au wedge bonding to Au-Ge pads and Al/Au wedge bonding to Au pads on the mounting chip. However, the NTD Ge to the Au-Ge pads is the most crucial and is required to be fabricated with perfection to overcome the Schottky barrier and to provide a truly ohmic contact.

The resistance data of NTD Ge samples B, D, E, F, G acquired by AVS resistance bridge in the temperature range of 20 mK to 400 mK are shown in Figure 4.18. The heavily doped sample B hardly shows any change in

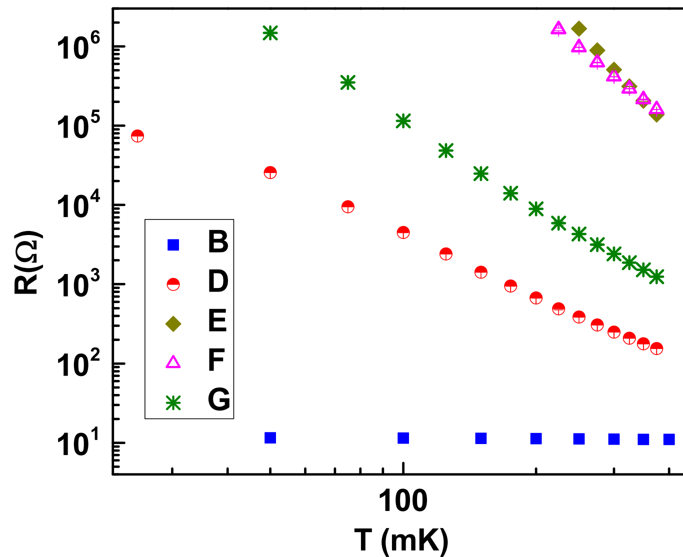

Figure 4.18: Resistance as a function of temperature for various NTD Ge samples, measured using AVS resistance bridge.

the resistance with respect to temperature, proving its metallic nature. The ohmic resistance of sample E measured by NI-PXI is analysed to fit the Mott

law (Equation 1.11) and the corresponding plot is shown in Figure 4.19. The

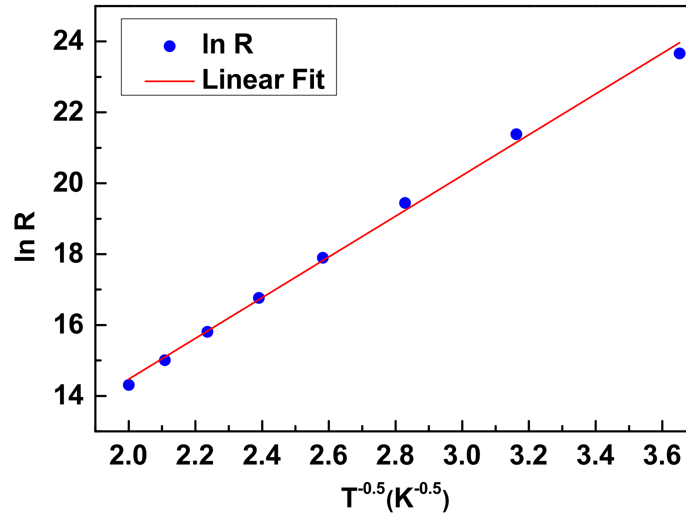

Figure 4.19: Linear fit of the logarithmic resistance of NTD Ge E with $T^{-0.5}$ till 75mK.

linear fit of the Mott's plot gives an intercept of 2.26(0.01) and a slope of 6.04(0.05). These fitting values are used to extract the parameters R_0 and T_0 for the sample E and are estimated as 9.6(0.1) and 36.5(0.6), respectively.

4.4 Summary

The irradiated Ge wafers were annealed and fabricated into NTD Ge sensors. The contact pads on NTD Ge were made using Au-Ge alloy and the thermal stability of the contact pad on NTD Ge were examined with an indigenously made cryo insert. The carrier concentration was experimentally estimated using Hall probe measurement and the values at 77 K were

found to be similar to that of estimated from reactor power data. Saturation of (Kapitza) resistance in NTD Ge samples at a low temperature can be overcome by mounting the samples directly on the Cu base. The crucial electrical interface: NTD Ge to Au-Ge pad has to be carefully made to overcome the Schottky barrier in the sensor at very low temperature. The heavily doped NTD Ge sample B ($\Phi_{th} > 10^{19}/cm^2$) hardly shows any change in the resistance with respect to temperature, proving its metallic nature. The NTD Ge samples with carrier concentration in the range 0.5 – 1 x $10^{17}/cm^3$ are found to be suitable for the sensor development. Preliminary measurements on resistance of sample E ($\Phi_{th} \sim 2 \times 10^{18}/cm^2$) measured by NI-PXI showed the electrical contact to be ohmic and moreover the data followed the Mott law with α equal to 0.5.

Chapter 5

Summary and Future Outlook

5.1 Summary

The process of single beta decay is forbidden in certain nuclei either due to energy or spin. Such nuclei can undergo double beta decay (DBD), a second order weak interaction. If the neutrino is a massive Majorana particle, in the case of nuclei undergoing DBD, there is a possibility of virtual annihilations of the two neutrinos leading to a neutrinoless double beta decay ($0\nu\beta\beta$) process. The experimental observation of $0\nu\beta\beta$ would violate total lepton number conservation and imply the neutrino to be a Majorana particle. Moreover, it can pave a way to physics beyond the standard model. The experimental signature of $0\nu\beta\beta$ decay is the constancy of sum energy of two electrons equal to Q value of the reaction. There are several experiments for the search of Majorana nature of the neutrino.

In India, efforts have been recently taken to search for $0\nu\beta\beta$ in ^{124}Sn. The INdia-based TIN (TIN.TIN) detector will be housed at the upcoming India based Neutrino Observatory (INO). This experiment involves the development of cryogenics bolometer detector operating at a milli-kelvin temperature to look for the thermal pulses corresponding to $Q_{\beta\beta}$ value of ^{124}Sn, which is 2292.64 $\pm$ 0.39 keV.

For a high energy resolution bolometric experiment, the performance of the sensor matters significantly. Neutron Transmutation Doped (NTD) Ge sensor is an optimum sensor to employ at mK temperature for its mass production, reproducibility and simpler readout. Highly sensitive NTD Ge sensors can be fabricated by doping Ge wafers just below the Metal Insulator Transition (MIT) regime. NTD Ge sensors are produced by doping Ge wafers by neutron transmutation technique. In this technique, the Ge wafers are irradiated with thermal neutrons from a nuclear reactor and the wafer gets uniformly doped. Indigenous development of NTD Ge sensor by irradiating Ge wafers in the Dhruva reactor facility at Bhabha Atomic Research Centre (BARC) has been initiated.

Semiconductor grade Ge wafers of cleavage planes $< 111 >$ (0.4 mm thick, $\rho \sim 30\ \Omega$ cm) and $< 100 >$ (1 mm thick, $\rho \geq 35\ \Omega$ cm) were taken for fabricating NTD Ge sensors. The isotopic abundance of the Ge samples was obtained with TOF-SIMS technique at BARC. Neutron irradiation has

been carried out on Ge samples placed in quartz tube/Al foil, with thermal neutron fluence in the range 1.8×10^{18} to $1.4 \times 10^{19}/\mathrm{cm}^2$ at Dhruva reactor, BARC.

During irradiation the exposure to high neutron dose can lead to radioactive contamination of Ge sensors due to surface impurities and other sources, even if starting material is of high purity (5N). Such trace radioactivity in sensors can produce significant background for rare event studies like DBD. Therefore to study and minimize the production of relatively long lived impurities in NTD Ge, radioactive impurity studies have been performed on the irradiated Ge wafers. The samples were spectroscopically studied for impurities in the low background counting setup (TiLES) and all peaks in the γ-spectra were identified. Chemical etching of the surface removed most of the long lived impurities, indicating that these impurities can arise either from residual surface contamination of the sample or due to diffusion during irradiation from the sample capsule environment. Generally the samples loaded in the quartz tube were found to have lower radioactivity than those wrapped in Aluminium. Spectroscopic studies of the Ge sample sealed in quartz tube did not show significant improvement in the level of radioactive impurities. Preliminary results of Ge samples etched prior to irradiation have shown promising results. The chemical etching after irradiation does not affect the performance of the sensor but is desirable even

from thermometry consideration since radioactive impurities can act as a standing heat load at mK temperature. For the desired neutron fluence of $1-5 \times 10^{18}$/cm^2, removal of 50 μm surface layer is found to be adequate. The observed radioactive impurities ~ 1 Bq/g in the bulk Ge, estimated after chemical etching of the samples, implies that a cooldown period of ~ 2 years would be necessary before sensors made from these samples can be used in rare decay studies requiring ultra low background (≤ 1 mBq/g).

The Ge samples were exposed to neutrons having a broad range of energies (< 0.625 eV to 10 MeV) during irradiation, since reactor neutrons are not mono-energetic. High energy neutrons, in particular, can cause damage to the lattice structure of the crystal. The dopant atom in interstitial positions cannot contribute to the total number of carrier concentration. Thus, defects created during the irradiation can significantly affect the performance of the sensor at low temperature. To study the fast neutron induced defects Positron Annihilation Lifetime Spectroscopy (PALS) and Channeling technique were employed. The PALS measurements indicated monovacant type defects for all irradiated samples, whereas the channeling studies revealed no significant defects for fast neutron fluence up to $\sim$ 4 x $10^{16}/\mathrm{cm}^2$. These fast neutron induced defects were observed in the irradiated samples even after about 4 - 8 months of irradiation. It is shown that vacuum annealing

at 600 $^{\circ}$C for $\sim$ 2 hours is sufficient to recover the damage in the irradiated samples, as verified from both PALS and channeling.

The irradiated Ge wafers were annealed and fabricated into NTD Ge sensors. The contact pads on NTD Ge were made using Au-Ge alloy and the thermal stability of the contact pad on NTD Ge were examined with an indigenously made cryo insert. The carrier concentration was experimentally estimated using Hall probe measurement and the values at 77 K were found to be similar to that of estimated from reactor power data. Saturation of (Kapitza) resistance in NTD Ge samples at the low temperature can be overcome by mounting the samples directly on the Cu base. The heavily doped NTD Ge sample B ($\Phi_{\mathrm{th}} > 10^{19}/\mathrm{cm}^2$) hardly shows any change in the resistance with respect to temperature, proving its metallic nature. The NTD Ge samples with carrier concentration in the range 0.5 – 1 x $10^{17}/\mathrm{cm}^3$ are found to be suitable for the sensor development. Preliminary measurements on resistance of sample E ($\Phi_{\mathrm{th}} \sim 2 \times 10^{18}/\mathrm{cm}^2$) measured by NI-PXI showed the electrical contact to be ohmic and moreover the data followed the Mott law with α equal to 0.5.

5.2 Future Outlook

To employ the NTD Ge sensors in the rare event $0\nu\beta\beta$ bolometric experiment, the bulk radioactive impurity should be minimized. This can be achieved by using detector grade Ge wafers as the starting material for sensor production. To reduce the surface impurities due to mechanical lapping/polishing, the Ge samples can be deeply etched prior to irradiation. For an accurate estimation on neutron fluence at the Ge sample site in the nuclear reactor, the reliable neutron monitors like Zr (thermal), Cd (epithermal) and Fe (fast) can be used. During fabrication, the crucial electrical interface: NTD Ge to Au-Ge pad has to be carefully made to overcome the Schottky barrier in the sensor at very low temperature. Further improvement on electrical contacts can be done by etching the irradiated Ge sample mechanically in addition to chemical etching, before making the contact pads. The measure of carriers get activated as a function of annealing temperature can be performed by carrying out Hall Effect measurement on samples annealed at various temperature. Specific heat measurement of NTD Ge sensors with various dopant level can also be carried out to optimize the minimal specific heat contribution of the sensor to the bolometer.

In a bolometric experiment, the energy incident (produced) on (in) the absorber is measured as the temperature change in the sensor. The temperature change in the bolometer mainly depend on the total specific heat of the

bolometer (C_{tot}) and the thermal conductivity of the weak heat link (G_w). The ratio of C_{tot}/G_w determines the detector time constant (τ_d). At very low temperature, there is a possibility for the electron and phonon of the temperature sensor to decouple. In such case, there is an additional internal time constant τ_{e-ph} of the sensor present in the system. Knowledge of this τ_{e-ph} is crucial in terms of the detector performance. In general τ_{e-ph} should be α (logarithmic sensitivity) times less than that of the detector time constant, to avoid the additional noise due to thermodynamical fluctuations between electron and phonon bath.

Glossary A

Glossary

Glossary of terms / acronyms (in order of appearance in the chapters).

$0\nu\beta\beta$: Neutrinoless double beta decay

$2\nu\beta\beta$: Two neutrino double beta decay

NTD Ge : Neutron transmutation doped Ge

BARC : Bhabha Atomic Research Centre

TES : Transition edge sensor

MMC : Magnetic micro calorimeters

MKID : Multiplexed Kinetic Inductance Detectors

VRH : Variable ange hopping

SQUID : Superconducting quantum interference device

MIT : Metal-insulator transition

INO: India-based Neutrino Observatory

TIN.TIN : The INdia-based TIN detector

TOF-SIMS : Time Of Flight Secondary Ion Mass Spectroscopy

SIMS : Secondary Ion Mass Spectroscopy

TiLES : Tifr Low background Experimental Setup

TIFR : Tata institute of fundamental research

FPGA : Field Programmable Gate Arrays

MC : Monte Carlo

REC : Radioactive Electron Capture

EDAX : Energy Dispersive X-ray Analysis

HF : Hydrofluoric acid

H_2O_2 : Hydrogen peroxide

CFDR : Cryogen Free Dilution Refrigerator

PALS : Positron Annihilation Lifetime Spectroscopy

TAC : Time to Amplitude Converter

ADC : Analog to Digital Converter

RBS : Rutherford Back Scattering

PARAS : Pelletron Accelerator RBS-AMS Systems

IUAC : Inter University Accelerator Centre

DAQ : Data Acquisition system

PID : Proportional, Integral and Derivative values

BIBLIOGRAPHY

[1] References to early literature on the subject can be obtained in K Winter (ed): Neutrino Physics (Cambridge University Press 1991).

[2] For an English translation of the text of this letter, see Pauli's article in Ref.[1].

[3] C. L. Cowan, F. Reines, F. B. Harrison, H. W. Kruse, A. D. McGuire, Science **124** (1956) 103.

[4] C. S. Wu et al., Physical Review **105** (1957) 1413.

[5] K. Nakamura and S. T. Petcov, 'Neutrino Masses, Mixing and Oscillations' in J. Beringer et al. (Particle Data Group), Phys. Rev., D **86** (2012) 010001.

[6] M. Goeppert-Mayer, Phys. Rev. **48** (1935) 512.

[7] W. Furry, Phys. Rev. **56** (1939) 1184.

[8] C. Giunti and C.W. Kim, 'Fundamentals of Neutrino Physics and Astrophysics', Oxford UP (2007) Print.

[9] A. Barabash, arXiv:1403.2870 [nucl-ex]

[10] V. Nanal, EPJ Web of Conferences **66** (2014) 08005.

[11] D.A. Nesterenko et al., Physical Review C, **86** (2012) 044313 .

[12] S.K. Agarwal, C.G. Karhadkar, A.K. Zope, Kanchhi Singh, Nuclear Engineering and Design **236** (2006) 747.

[13] S.P. Langles, Proc. American Metrol. Soc. **2** (1881) 184.

[14] S.P. Langles, Nature **25** (1881) 14.

[15] A. L. Woodcraft, R. V. Sudiwala, E. Wakui, C. Paine, Journal of Low Temperature Physics **134** (2004) 925.

[16] Adam L. Woodcraft, Nuclear Instruments and Methods in Physics Research Section A **604** (2009) (1-2):30-33.

[17] K. Uhlig, Journal of Physics: Conference Series **400** (2012) 052039.

[18] H.K. Onnes, Commun. Phys. Lab. Univ. Leiden **12** (1911) 120.

[19] D. H. Andrews, Am. Phil. Soc. Year Book (1938) p. 132

[20] D. H. Andrews, W. F. Brucksch, Jr., W. T. Ziegler and E. R. Blanchard, Phys. Rev. **59** (1941) 1045.

[21] D. H. Andrews, W. F. Brucksch, W. T. Ziegler, and E. R. Blanchard, Rev. Sci. Instrum. **13** (1942) 281.

[22] W. S. Boyle and K. F. Rogers, Jr., J. Opt. Sot. Am. **49** (1959) 66.

[23] F. J. Low, J. Opt. Sot. Am. **51** (1961) 1300.

[24] B.I. Shklovskii, A.L. Efros, Electronic Properties of Doped Semiconductors, Springer Publication (1984).

[25] GUDDEN, B., and SCHOTTKY, W., Z. tech. Physik **16** (1935) 323.

[26] G. Bush and H. Labhart, Helv. Phys. Acta **19** (1946) 463.

[27] C. S. Hung and J. R. Gliessman, Phys. Rev. **79** (1950) 726.

[28] A.L. Efros, B.I. Shklovskii, J. Phys. C: Solid State Physics **8** (1975) L49.

[29] K. M. ltoh, W. L. Hansen, J. W. Beeman, E. E. Haller, J. W. Farmer, V. I. Ozhogin, Journal of Low Temperature Physics **93** (1993) 307.

[30] J. Zhang et al., Phys. Rev. B 48, 2312 (1993).

[31] A.E. Lita, D. Rosenberg, S. Nam, A.J. Miller, D. Balzar, L.M. Kaatz, and R.E. Schwall, IEEE TRANSACTIONS ON APPLIED SUPERCONDUCTIVITY **15** (2005) 3528.

[32] T.C. Chen, F.M. Finkbeiner, A. Bier and B. DiCamillo, Supercond. Sci. Technol. **12** (1999) 840.

[33] W. Seidel: Diploma Thesis, Technische UniversitÂ¨at MÂ¨unchen 1986, unpublished.

[34] E. Umlauf, M. BÂ¨uhler: Proc. Symp. Supercon. and Low-Temp. Detectors, eds. G. Waysand and G. Chardin, 309 (North-Holland, Amsterdam 1989).

[35] S.R. Bandler, C. Enss, R.E. Lanou, H.J. Maris, T. More, F.S. Porter, and G.M. Seidel: J. Low Temp. Phys. **93** (1993) 709 .

[36] A. Fleischmann, M. Link, T. Daniyarov, H. Rotzinger, C. Enss, G.M. Seidel, Nuclear Instruments and Methods in Physics Research Section A **7 520** (2004) 27.

[37] P.K. Day, H.G. LeDuc, B.A. Mazin, A. Vayonakis and J. Zmuldzinas, Nature **425** (2003) 817.

[38] E. Pasca, E. Oliveri, G. Ventura, M. Barucci, L. Risegari, J. Beeman, Proc. of 8th Int. Conf. Adv. Technol. Part. Phys. **2** (2004) 93.

[39] K. M. Itoh et al., Phys. Rev. Lett. **77** (1996) 4058.

[40] N.K. Mondal, Pramana **79** (2012) 1003.

[41] V. Sanglard et al., Phys. Rev. D **71** (2005) 122002 1.

[42] P. Gorla, Journal of Physics: Conference Series **375** (2012) 042013 1.

[43] E.E. Haller, Infrared Phys. **25** (1985) 257.

[44] K. M. ltoh, E. E. Haller, W. L. Hansen, J. W. Beeman,J. W. Farmer, A. Rudnev, A. Tikhomirov, V. I. Ozhogin, Appl. Phys. Lett., **64** (1994) 2121.

[45] A. Alessandrello, C. Brofferio, D.V. Camin, O. Cremonesi, E. Fiorini, A. Giuliani, M. Pavan, G. Pessina, E. Previtali, L. Zanotti, Nuclear Instruments and Methods in Physics Research Section B **93** (1994) 322.

[46] http://www.universitywafer.com.

[47] Alexander Axelevitch, Gady Golan, Electronics and Energetics **26** (2013) 187.

[48] S. Mathimalar et. al., Nuclear Instruments and Methods in Physics Research Section A **774** (2015) 68.

[49] N. Dokania, V. Singh, S. Mathimalar, V. Nanal, S. Pal, R.G. Pillay, Nuclear Instruments and Methods in Physics Research Section A **745** (2014) 119.

[50] Bruno W. Schueler, Microsc. Microanal. Microstruct. **3** (1992) 119.

[51] K.G.Bhushan, R. Mukundhan and S.K. Gupta, Solid State Physics **57** (2012) .

[52] K.G. Bhushan, R. Mukundhan and S K. Gupta, AIP Conf. Proc. **1512** (2013) 680.

[53] http://www.nndc.bnl.gov.

[54] M. Berglund, M.E. Wieser, Isotopic compositions of the elements 2009 (IUPAC Technical Report), Pure Appl. Chem. **83** (2011) 397.

[55] R.B. Firestone, V.S. Shirley, Table Of Isotopes **1** 8th Edition.

[56] B.L. Saraf, J. Varma, C.E. Mandeville, Physical Review **91** (1953) 1216.

[57] N. Cerniglia and P. Wang, Journal of The Electrochemical Society **109** (1962) 508.

[58] John C. Russ, Fundamental of Energy Dispersive X-ray Analysis, Butterworth-Heinemann Ltd (1984).

[59] Ling Y. Wei, J. Phys. Chem. Solids **18** (1961) 162.

[60] http://adsem.com/index.html.

[61] S.R. Elliott, V.E. Guiseppe, and B.H. LaRoque, R.A. Johnson, S.G. Mashnik, Physical Review C **82** (2010) 054610.

[62] H. C. Schweinler, Journal of Applied Physics, **30** (1959) 1125.

[63] R. R. Hasiguti, Defects and Radiations Effects in Semiconductors (1980) 46.

[64] K. Kuriyama, M. Yahagi, K. Iwamura, Y. Kim, C. Kim, Journal of Applied Physics, **54** (1983) 673.

[65] N. P. Palaio, S. J. Pearton, E. E. Haller, Journal of Applied Physics, **55** (1984) 1437.

[66] S. Mathimalar et. al., Nuclear Instruments and Methods in Physics Research Section B **345** (2015) 33.

[67] G. Fabri, G. Poletti, G. Randone, Physical Review **151** (1966) 356.

[68] P. Kirkegaard, N.J. Pedersen, M. Eldrup, PATFIT-88, Risϕ-M-2740 (Roskilde, Denmark, 1989).

[69] R.K. Rehberg, H.S. Leipner, Positron Annihilation in Semiconductors - Defect Studies, Springer Publication (1999).

[70] S. Mathimalar, V. Singh, N. Dokania, V. Nanal, R. G. Pillay, S. Pal, S. Ramakrishnan, A. Shrivastava, Priya Maheshwari, P.K. Pujari, S. Ojha, D. Kanjilal, K.C. Jagadeesan, S.V. Thakare, IEEE WOLTE conference, (2014) 10.1109/WOLTE.2014.6881014.

[71] D. S. Gemmell, Rev. Mod. Phys. **46** (1974) 129.

[72] M. Satoh, K. Kuriyama, Journal of Applied Physics **67** (1990) 3890.

[73] http://www.iuac.res.in/accel/paras.

[74] F. J. Morin, Physical Review **93** (1954) 62.

[75] V. Singh, S. Mathimalar, N. Dokania, V. Nanal, R.G. Pillay, S. Ramakrishnan, Pramana **81** (2013) 719.

[76] E.T. Swartz and R.O. Pohl, Review of Modern physics **61** (1989) 605.

[77] J.P. Shepherd, Rev Sci Instrum. **56** (1985) 273.